https://doi.org/10.5194/egusphere-2026-3371
Preprint. Discussion started: 18 November 2026
© Author(s) 2026. CC BY 4.0 License.

# A Regional Subseasonal-to-Seasonal (S2S) Ocean-Atmosphere Forecast System for Peru and Ecuador

Ivonne Montes[1,2], Berlin Segura[1], Fiorela Castillón[1], Roger Manay[1], Fernando Campos[3], Boris Dewitte[4,5,6], Katerina Goubanova[4,7], Veronique Garcon[8], Didier Gazen[9], Kobi Mosquera[1], Ken Takahashi[1]

[1] Instituto Geofísico del Perú (IGP), Lima, Peru
[2] Universidad Ingeniería y Tecnología (UTEC), Lima, Peru
[3] Centro de Investigación Científica y de Educación Superior de Ensenada (CICESE), Ensenada, B.C., Mexico
[4] Centro de Estudios Avanzados en Zonas Áridas (CEAZA), Coquimbo, Chile
[5] Departamento de Biología Marina, Facultad de Ciencias del Mar, Universidad Católica del Norte, Coquimbo, Chile
[6] CECI, Université de Toulouse III, CERFACS/CNRS, Toulouse, France
[7] Météo France, Toulouse, France
[8] CNRS - Institut de Physique du Globe de Paris, Paris, France.
[9] Laboratoire d'Aérologie, Université de Toulouse, CNRS, UPS, Toulouse, France

*Correspondence to*: Ivonne Montes (imontes@igp.gob.pe)

**Abstract.** Reliable climate prediction across timescales is essential for regions strongly impacted by ENSO variability, such as the northern coasts of Peru and Ecuador, where intense rainfall and flooding can have socio-economic impacts. Although existing subseasonal-to-seasonal (S2S) prediction systems based on global models provide valuable climate information, they still suffer from mean-state biases and insufficient spatial resolution to represent key regional processes, including coastal upwelling and mesoscale air-sea interactions. Here, we present IGP RESM-COW, a regional coupled ocean-atmosphere Earth system model designed for the eastern tropical Pacific and the Peruvian/Ecuadorian domain. A long-term simulation covering 2001-2025 shows that the model reproduces the main features of regional oceanic and atmospheric variability, including SST gradients, coastal upwelling, and the seasonal cycle, although with reduced performance over areas of complex topography. In forecast mode, 34 hindcasts initialized between September 2022 and June 2025 with lead times up to 7 months were evaluated. The system exhibits forecast skill comparable to global models in terms of anomaly correlation, while reducing forecast errors, particularly in the Niño 1+2 region and along the Peruvian coast. These improvements are associated with a better representation of SST anomaly amplitude and spatial patterns. At subseasonal timescales, the model maintains predictive skill for SST anomalies up to three weeks, especially in the northern coast, highlighting its potential for short-term preparedness applications. Overall, IGP RESM-COW provides a robust framework for monitoring and forecasting ocean-atmosphere variability in the eastern tropical Pacific, demonstrating the added value of regional coupled modelling in eastern boundary upwelling systems.

## 1 Introduction

https://doi.org/10.5194/egusphere-2026-3371
Preprint. Discussion started: 18 November 2026
© Author(s) 2026. CC BY 4.0 License.

El Niño, characterized by the anomalous warming of the equatorial Pacific ocean, is a climatic phenomenon that exerts severe impacts on Peru. Its effects are most evident through intense rainfall, floods, and landmass movements along the coast, as well as droughts across the Andes and the Amazon (Sulca et al., 2018). In Peru, the warm phase of the El Niño–Southern Oscillation (ENSO)—El Niño—generates the most severe consequences, altering rainfall patterns not only along the northern coast but also in the Andean highlands and the Amazon basin (Takahashi, 2022; Lagos et al., 2008; Lavado-Casimiro & Espinoza, 2014; Sulca et al., 2018). These anomalies strongly affect the socioeconomic system (Callahan & Mankin, 2023; Cai et al., 2020), causing damage to infrastructure (Machuca et al., 2014), agriculture (Heino et al., 2018), fisheries (Bertrand et al., 2020), and public health (Yglesias-González et al., 2023), among other sectors.

Both El Niño and its cold counterpart, La Niña, exhibit diverse manifestations and dynamics (Capotondi et al., 2020). Particularly relevant for Peru are extreme global El Niño events in the eastern Pacific—such as those of 1982–1983 and 1997–1998—as well as extreme coastal El Niño events, exemplified by 1925, 2017, and 2023. From a physical perspective, global El Niño events, one of the dominant modes of climate variability worldwide, which fundamentally depends on ocean–atmosphere interactions across the tropical Pacific (McCreary & Anderson, 1991) referred to as the Bjerknes feedback. Extreme events take place when there is a non-linear amplification of this feedback in the eastern Pacific that involve either atmospheric (Takahashi & Dewitte, 2016; Takahashi et al., 2018) or oceanic (Jin et al., 2003) processes. By contrast, coastal El Niño events, such as those of 1925, 2017, and 2023, although involving precursor signals at basin scale (Martinez-Villalobos et al., 2024), involve regional-scale ocean–atmosphere interactions limited to the region off the coast of Peru, which is referred as a coastal Bjerknes feedback. In contrast with basin-scale events that can last several seasons, they reach their peak in a few months with little persistence (Takahashi & Martinez, 2017; Echevin et al., 2018; Peng et al., 2019; 2024)

Forecasting El Niño and La Niña events—particularly along the Peruvian coast—requires accurate representation of eastern Pacific ocean–atmosphere interactions. Yet, the predictive skill of global climate models in this region is generally lower than in the central Pacific (Rivera-Tello et al., 2023), likely due, at least in part, to systematic warm and wet climatological biases near the Peruvian coast (e.g., Ding et al., 2020). To improve forecast accuracy, especially at lead times useful for decision-making (i.e. a few months), it is essential to develop models that realistically capture regional-scale physical processes in the eastern Pacific. This is particularly critical for anticipating extreme global El Niño events (e.g., 1982–1983 and 1997–1998) and extreme coastal events (e.g., 1925, 2017 and 2023).

Existing international forecast bulletins primarily focus on the prediction of basin-scale El Niño events (e.g., NOAA), with limited attention to regional variability across the tropical Pacific. Some recent bulletins have begun to address coastal El Niño–like phenomena in other eastern boundary upwelling systems (e.g., Benguela or California coastal El Niño; see the SINTEX advisory), but they suffer limitations associated with the use of low-resolution global coupled model. Currently there is no international advisory for coastal El Niño events off Peru. This represents a critical gap for Peru and other countries in the region (Ecuador, Chile). Current regional El Niño advisories are provided by a national committee named ENFEN (Comisión Multisectorial encargada del Estudio Nacional del Fenómeno “El Niño”) established by Resolución Ministerial 120-77-PM/ONAJ in 1977 and reorganized by Resolución Suprema Nº 053-97-PE in 1997. ENFEN analyzes oceanic and atmospheric conditions using national and international observational datasets together with forecasts from global climate models and issues El Nino bulletins and technical reports tailored to the Peruvian coast. This initiative has been key for advancing predictive capabilities of extreme climate events with impacts on Peru, as well as for establishing a roadmap for relevant modeling activities (Mosquera, 2014; Urbina & Mosquera, 2020; Rivera-Tello et al., 2023).

Recent efforts include the development of a regional ocean-atmosphere coupled model as a basis for a regional subseasonal to seasonal (S2S) forecasting system. This approach provides substantially higher spatial resolution than global prediction systems, allowing a more realistic representation of coastal circulation, air-sea interactions, and mesoscale processes

https://doi.org/10.5194/egusphere-2026-3371
Preprint. Discussion started: 18 November 2026
© Author(s) 2026. CC BY 4.0 License.

that are critical for understanding the evolution of extreme coastal events. Previous studies over South America have shown that regional coupled systems improve the representation of SST, atmospheric circulation, and Humboldt upwelling system relative to uncoupled regional models (e.g., Ordoñez et al., 2024). In particular, improved representation of nearshore dynamics is essential for evaluating hazards such as coastal flooding, anomalous sea levels, storm surges, and enhanced river runoff associated with climate variability and El Niño events. Furthermore, the regional modeling system provides a foundation for integrating biogeochemical components, enabling the evaluation of ecosystem responses and coastal impacts such as harmful algal blooms. Overall, this regional S2S modeling approach is expected to enhance predictive capability at local scale while improving the mechanistic understanding of coastal extremes and their associated physical and biogeochemical processes (Vitart et al., 2012; 2017). These advances have stimulated further modeling efforts aimed at increasing confidence in regional forecasts. The work presented here, led by the IGP, directly contributes to this objective by enhancing predictive capabilities at the regional scale.

As a pioneer in numerical climate modeling in Peru, the IGP contributes operational forecasts based on both international climate models and its own tools, including an equatorial ocean wave prediction model (Mosquera, 2014; Urbina & Mosquera, 2020) and an artificial intelligence–based El Niño forecasting system (Rivera-Tello et al., 2023). Building on this experience, and in the collaboration with the French National Research Institute for Sustainable Development (IRD), the IGP has developed a regional coupled ocean–atmosphere Earth System model (Segura & Montes, 2021; Montes et al., 2023; Cirano et al., 2024), referred to as the IGP RESM-COW, which operates on the Institute's high-performance computing system (Montes et al., 2016). This regional model, driven by global data, is capable of representing key local physical processes and has successfully reproduced conditions observed during the 2017 and 2023 coastal El Niño. Consequently, it offers the potential to deliver improved forecasts of El Niño and La Niña events for both the eastern Pacific and the Peruvian territory. This effort underscores Peru's commitment to advancing predictive capabilities and strengthening resilience in the face of one of the most influential climate phenomena worldwide.

This paper is structured as follows. Section 2 provides a detailed description of the model configuration. Section 3 examines the model performance, including its representation of annual, seasonal, and interannual variability, as well as its forecasting skill. Conclusions are presented in Section 4.

## 2 A regional coupled ocean-atmosphere model

### 2.1 Coupled model description

The coupled regional ocean-atmosphere numerical model IGP RESM-COW was developed based on the CROCO (Coastal and Regional Ocean Community model) oceanic model version 2.0 (Auclair et al., 2022), the WRF (Weather Research and Forecasting model) atmospheric model version 4.0 (Skamarock et al., 2019) and the OASIS3-MCT (Ocean-Atmosphere-Sea-Ice-Soil Model Coupling Toolkit) coupler version 5 (Craig et al., 2017; Valcke et al., 2021).

CROCO is a next-generation ocean model, developed within the framework of ROMS (Regional Oceanic Modeling System; Shchepetkin and McWilliams, 2005), specially designed to simulate fine-scale circulation processes and their interactions with larger-scale dynamics. WRF, in turn, is a flexible, portable, and computationally efficient atmospheric simulation system optimized for parallel computing platforms (Skamarock et al., 2019). The primary role of OASIS is to exchange and interpolate coupling fields between the CROCO and WRF models. In this configuration, the data exchange frequency between the coupled models is set to 1 h. WRF provides CROCO with hourly averages of zonal and meridional wind stress, shortwave and longwave radiative fluxes, and freshwater fluxes. Conversely, CROCO supplies WRF with the hourly average of sea surface temperature (SST). The integration time steps are 90s for WRF and 900s for CROCO. Since the ocean and atmospheric domains are not identical, the OASIS coupler interpolates data between WRF and CROCO grids using bilinear spatial interpolation.

https://doi.org/10.5194/egusphere-2026-3371
Preprint. Discussion started: 18 November 2026
© Author(s) 2026. CC BY 4.0 License.

## 2.2 Model configuration

*Ocean model configuration*

The ocean model configuration used in this study builds upon a previously developed and validated setup described by Montes et al. (2011). The model domain extends over the eastern tropical Pacific, from 22°S to 4°N and from 94°W to the South American coast, with a horizontal resolution of ~12 km and 32 terrain-following vertical levels (Figure 1), which is refined in the upper ocean. Bottom topography is derived from the ETOPO2 dataset (2′ resolution; Smith and Sandwell, 1997).

*Atmospheric model configuration*

The model domain spans the region from 23°S to 4°N and from 97°W to 66°W (Figure 1). The horizontal resolution is ~30 km, with 32 terrain-following vertical levels. The model configuration employs the planetary boundary layer scheme of Nakanishi and Niino (2006; PBL5), the microphysics scheme of Hong and Lim (2006; MP6), the Kain-Fritsch cumulus parametrization (Kain, 2004), and the NOAH land surface scheme (Chen et al., 1996).

The same coupled model configuration described above is used for two types of simulations: (1) a long-term coupled integration covering 2000-2025, designed to reproduce the observed evolution of the ocean-atmosphere system under realistic boundary conditions (see section 2.2.1), and (2) a set of forward forecast integrations with lead times up to seven months, initialized with boundary conditions derived from global forecasting systems (see section 2.2.2). The model configuration (domains, resolution, coupling strategy, and physical parametrization) is identical in both experiments. The differences between them arise only from the specification of initial and lateral boundary conditions. The long-term coupled integration also provides dynamically consistent initial conditions for the forecast run.

### 2.2.1 Long-term coupled simulation

In this simulation, the ocean component was initialized in January 2000 using the oceanic state from Montes et al. (2011) simulation, which was shown to be dynamically balanced. That earlier configuration was demonstrated to realistically reproduce many aspects of the mean oceanic circulation in the far eastern Pacific, including the off-equatorial meridionally confined subsurface currents (Tsuchiya jets) and the vertical structure of the Equatorial Undercurrent (EUC). Monthly varying variables from the Simple Ocean Data Assimilation Parallel Ocean Program (SODA-POP) reanalysis (Carton and Giese, 2008) were used to prescribe the open boundary conditions (north, west, and south) for horizontal currents, sea level, temperature and salinity during the period 2000-2015. For the subsequent years, boundary conditions were provided by global ocean data assimilation products: GLORYS12V1 (Jean-Michel et al., 2021) for 2016-2019 and PSY4QV3R1 (Lellouche et al., 2018; Le Galloudec et al., 2025) for 2020 to the present. On the other hand, the atmospheric component of the coupled system is forced with data from the NCEP FNL (Final Operational Global Tropospheric Analyses) at 6-hour intervals for the period 2000-2025. The WRF model is initialized from FNL fields at 00UTC on 1 January 2000, although the coupled integration effectively starts at 03 UTC, when the first SST field from CROCO is provided to WRF. Therefore, WRF exchanges surface heat fluxes, freshwater fluxes, and wind stress with CROCO throughout the coupled simulation.

https://doi.org/10.5194/egusphere-2026-3371
Preprint. Discussion started: 18 November 2026
© Author(s) 2026. CC BY 4.0 License.

### 2.2.2 Forecast experiments

In the forecast simulations, open boundary conditions for both the ocean and the atmospheric components are derived from Climate Forecast System (CFS, https://www.ncei.noaa.gov/products/weather-climate-models/climate-forecast-system). CFS is a global coupled prediction system developed by the National Centers for Environmental Prediction (NCEP) that simulates the interactions between the ocean, atmosphere, and land components, providing hourly outputs at a horizontal resolution of 0.5° (~56 km). Previous studies indicate that the subseasonal forecast skill of CFS for some fields of the tropical free atmosphere is generally limited to the first few weeks. For example, Weber and Mass (2017) showed that 500-hPa geopotential height and 200-hPa velocity potential rapidly lose skill beyond approx. 2 weeks as forecast errors saturate, while more slowly varying components such as sea surface temperature retain predictive skill for up to one month. This is particularly evident in the equatorial Pacific, including the Niño 1+2 region, where the model benefits from its ability to represent ENSO-related variability.

For the ocean component, CFS fields used to force CROCO in forecast mode include five variables: sea temperature, salinity, sea level, and zonal and meridional velocity fields (Table 1). For the atmospheric component, CFS fields used to force WRF include temperature, zonal and meridional wind components, geopotential height, relative humidity, and sea level pressure (Table 1). It is important to note that data employed correspond to the CFS 7-day rotating archives (https://nomads.ncep.noaa.gov/pub/data/nccf/com/cfs/prod/), which remain available for one week and contain complete forecast datasets extending up to seven months ahead for both the ocean and atmosphere.

Table 1. Variable extracted from the CFS used to force the coupled model

| Earth's System component | Variable | Unidades |
|---|---|---|
| Atmosphere | Temperature | K |
| | Zonal velocity | m $s^{-1}$ |
| | Meridional velocity | m $s^{-1}$ |
| | Geopotential height | m |
| | Relative humidity | % |
| | Sea-level pressure | Pa |
| Ocean | Temperature | °C |
| | Salinity | psu |
| | Zonal velocity | m $s^{-1}$ |
| | Meridional velocity | m $s^{-1}$ |
| | Sea level | m |

*Bias correction or climatological adjustment method*

Prior to their use as open boundary conditions for the forecast runs with the regional coupled model, the CFS forecast fields (both oceanic and atmospheric) undergo a climatological bias correction. This step is required because, in the eastern Pacific ocean, the raw CFS outputs exhibit significant drift and systematic errors, leading to overestimation or underestimation depending on the region considered. For instance, in the case of SST (Figure 1), a comparison between the CFS (at lead 0) and MERCATOR model climatologies reveals a warm bias of 2-3 °C off the Peruvian coast, although key dynamical features such

https://doi.org/10.5194/egusphere-2026-3371
Preprint. Discussion started: 18 November 2026
© Author(s) 2026. CC BY 4.0 License.

as coastal and equatorial upwelling remain clearly represented. Note that for this analysis, the global MERCATOR model is used because it incorporates a data assimilation system that integrates various observed data (Lellouche et al., 2021). This includes sea level anomalies from the Jason, Envisat, and GFO satellites, SST from CORIOLIS, temperature and salinity profiles from ARGO, and in situ measurements collected by drifting buoys, ships, and both global and regional research cruises (Brasseur et al., 2005; Lellouche et al., 2018a;b). In the case of surface winds, a comparison between CFS outputs and ASCAT (Advanced Scatterometer) satellite observations indicates an overestimation between 0.3 and 1 $ms^{-1}$ and, e.g., of about 1 -2 $ms^{-1}$ during 2022 (Figure 2b), accompanied by a poorly resolved pattern in the curl of wind stress (Figure 2a).

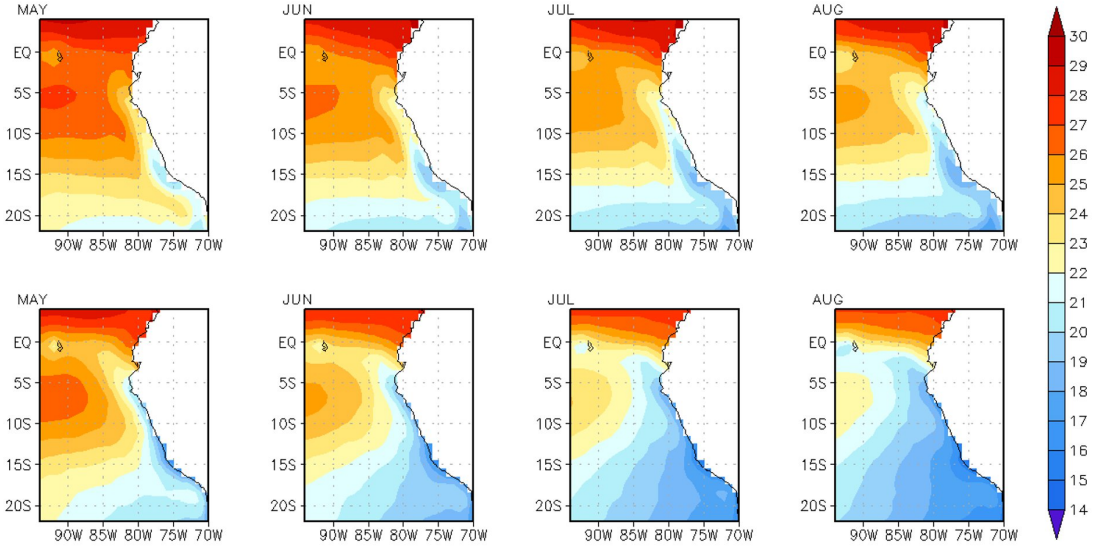



**Figure 1. Monthly mean sea surface temperature (°C) maps for May and August, calculated for the CFS lead-O climatology (Top) and the MERCATOR climatology (Bottom). These months are shown because they correspond to the period of strongest coastal upwelling and maximum meridional SST gradient in the southeastern tropical Pacific. Climatologies were used over the available periods for each dataset: 1982-2010 for CFS lead-0 and 1993-2019 for MERCATOR.**

https://doi.org/10.5194/egusphere-2026-3371
Preprint. Discussion started: 18 November 2026
© Author(s) 2026. CC BY 4.0 License.

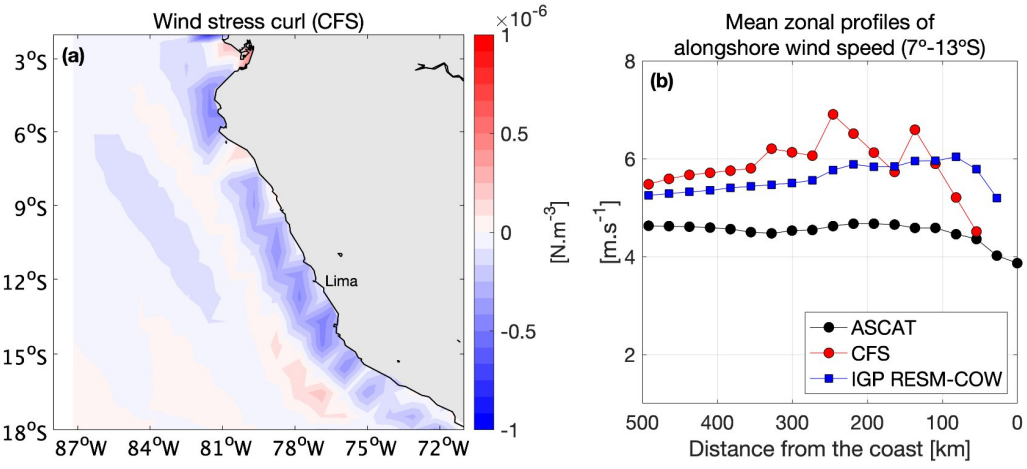



**Figure 2. (a) Mean wind stress curl computed from the CFS climatology (1982–2010, lead 0) over the Peruvian domain. (b) Mean zonal profiles of the alongshore wind speed (7°–13°S) as a function of distance from the coast, derived from ASCAT observations (black dots) and the CFS climatology (red dots). The IGP RESM-COW regional model output (blue squares) is included for reference. ASCAT and IGP RESM-COW climatologies correspond to the 2001–2025 period. Missing values near the coast reflect the absence of valid ocean points in the respective model grids.**

The climatological correction, also referred to as the bias-correction method, is applied to improve the consistency of CFS forecast data with observations. This is achieved by computing the climatological difference between observed and CFS fields and subsequently adding this correction term to the projected value (Soriano et al., 2019), such that:

$$T_{corr} = T_{forecast} + (T_{clim\text{-}obs} - T_{clim\text{-}CFS}) \quad (1)$$

Where $T_{forecast}$ represents each of the CFS forecast variables (see Table 1; e.g., SST, Figure 3, upper panel), $T_{clim\text{-}obs}$ is the observed climatology (MERCATOR 1993-2019 for the ocean and FNL 2008-2022 for the atmosphere), $T_{clim\text{-}CFS}$ corresponds to the CFS climatology (1982-2010), and $T_{corr}$ is the corrected variable (Figure 3, lower panel).

https://doi.org/10.5194/egusphere-2026-3371
Preprint. Discussion started: 18 November 2026
© Author(s) 2026. CC BY 4.0 License.

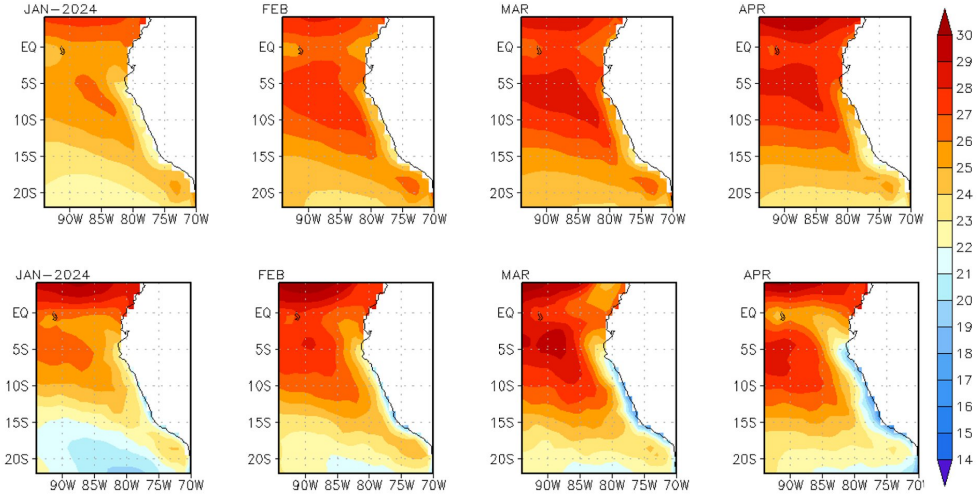



**Figure 3. Monthly mean SST (°C) maps from the CFS forecast model at lead 0 without (Top) and with (Bottom) climatological correction for January-April 2024.**

An important consideration is that CFS forecast errors increase with lead time. Since the CFS is initialized with analyzes close to observed states, its climatic bias emerges progressively as the forecast advances. Therefore, the correction must be applied separately for each forecast lead month. To achieve this, we computed the mean climatological error from retrospective CFS simulations for each initialization month and lead time. Considering 12 initialization months per year and up to 7 forecast months per run, a total of 12×7=84 climatological mean corrections were derived. This approach prevents the regional coupled model from being contaminated by the systematic biases of the CFS forecasts.

## 3 Model performance

To assess the skill of the IGP RESM-COW regional coupled ocean-atmosphere model, we evaluated its ability to reproduce observed variability at annual mean, seasonal, and interannual timescales, as well as its forecast skill (ACC and RMSE as a function of leadtime). Model outputs were contrasted with a range of observational and reanalysis datasets, allowing for a systematic quantification of biases and correlations. This approach provides insight into the model's capacity to resolve large-scale and regional processes relevant to the eastern tropical Pacific and the Peruvian territory.

### 3.1 Annual mean and seasonal variability

To assess the realism of the long-term coupled simulation under the annual mean and seasonal variability, we compared the model's climatology over the 2001-2025 period derived with three variables from satellite and observed data sources — SST from the OSTIA product (Operational Sea Surface Temperature and Ice Analysis), precipitation from the GPM (Global Precipitation Mission) product and PISCO (Peruvian Interpolation data of the SENAMHI's Climatological and hydrological Observations; Aybar et al., 2020), and winds from ASCAT — as well as with a reanalysis data source: low and upper level wind vector from the ERA5 (Fifth generation European Centre for Medium-Range Weather Forecasts (ECMWF) atmospheric reanalysis) product.

https://doi.org/10.5194/egusphere-2026-3371
Preprint. Discussion started: 18 November 2026
© Author(s) 2026. CC BY 4.0 License.

Figure 4 shows the annual mean SST climatology for the 2001-2025 period from the IGP RESM-COW model and the OSTIA product, together with their mean spatial bias. Overall, the model realistically represents the large-scale SST distribution of the eastern tropical Pacific, capturing the meridional temperature gradient, the equatorial cold tongue, and the band of relatively low SSTs along the Peruvian coast associated with the coastal upwelling. The simulated patterns and amplitudes are in close agreement with OSTIA SST over most of the domain; the model exhibits a small cold bias relative to OSTIA, with a domain-averaged difference of about -0.2 °C, indicating a robust representation of the regional surface thermal structure. The remaining differences are spatially organized and mainly confined to coastal and equatorial upwelling regions. Positive biases dominate the central-southern coastal region, with a maximum exceeding 1.6 °C near 12 °S in the vicinity of Punta San Juan, and weaker positive values extending northward along the coast to about 3 °S. In contrast, negative biases prevail north of about 12°S, with the strongest cold differences located along the northern Peruvian coast, off Tumbes, and the Gulf of Guayaquil. These localized discrepancies, confined to dynamically active coastal regions, do not alter the overall realism of the simulated climatology and highlight areas where further refinements of coastal processes may lead to additional improvements.

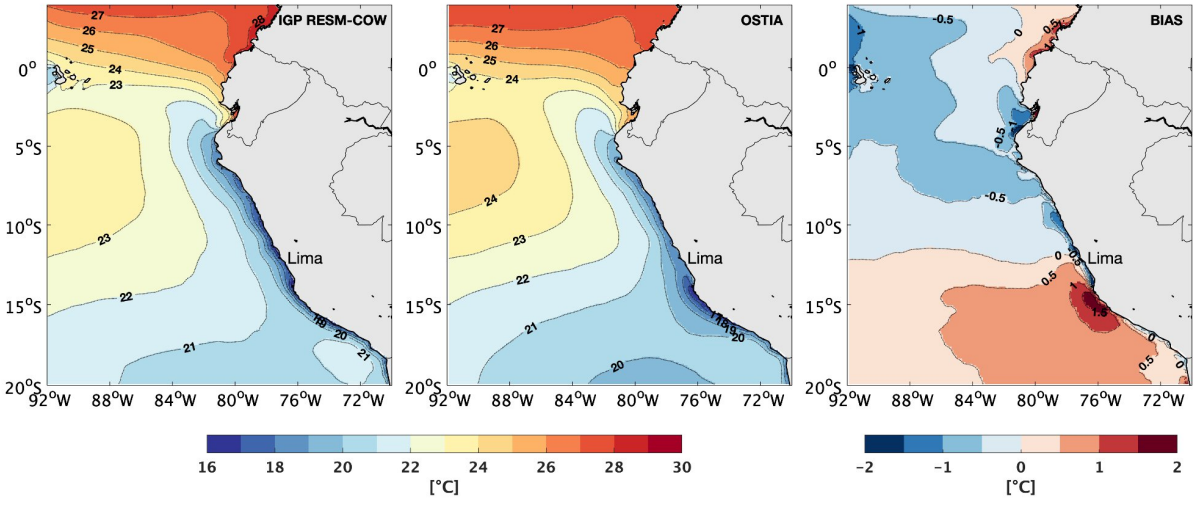



**Figure 4. Spatial distribution of the annual mean sea surface temperature (°C) climatology over the 2001-2025 period for the entire domain derived from the IGP RESM-COW model (left), the OSTIA product (middle), and their mean bias (right). The domain-average SST is 22.4 °C in the model and 22.6°C in OSTIA.**

Related to the wind stress, the coupled regional model reproduces the main characteristics of the near-surface circulation over the eastern tropical Pacific (Figure 5), including the predominantly equatorward alongshore flow off Peru, the offshore-directed wind component, and the large-scale meridional gradient in wind intensity. The comparison of the annual mean surface wind stress from the coupled regional model and ASCAT shows that the spatial structure and magnitude of the modeled wind stress are in close agreement with ASCAT over most of the domain, indicating that the coupled model realistically captures the regional wind forcing relevant to coastal upwelling and air-sea interactions (Figure 5). The RMSE shows relatively low values over the central offshore region and higher values mainly confined to the nearshore band and northern region, where coastal effects and atmospheric boundary-layer processes are known to introduce large uncertainties (e.g., Jacox et al., 2018). These results show the ability of the coupled model to provide a consistent and physically realistic representation of the surface wind field over the Humboldt Current System.

https://doi.org/10.5194/egusphere-2026-3371
Preprint. Discussion started: 18 November 2026
© Author(s) 2026. CC BY 4.0 License.

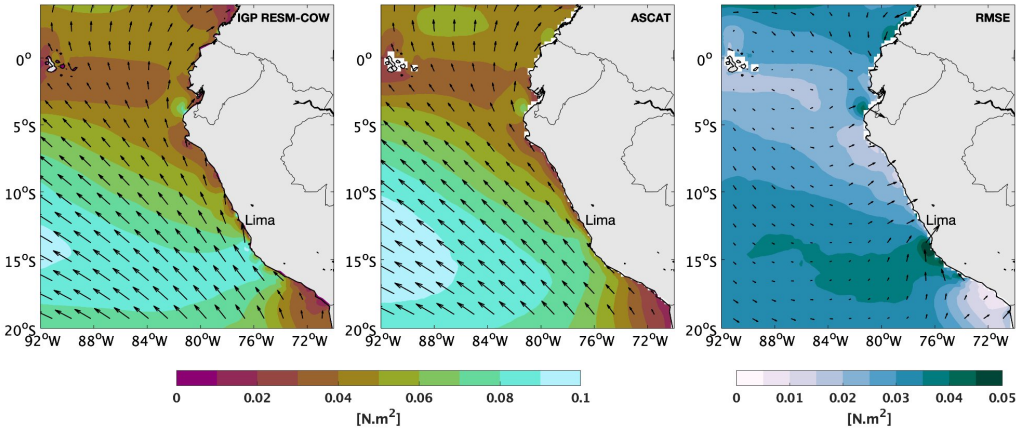



**Figure 5. Spatial distribution of the annual mean surface wind stress over the 2001-2025 period for the entire domain from the IGP RESM-COW model (left), the ASCAT product (central), and the Root Mean Square Error (RMSE) between observations and model results (right). In the latter, arrows indicate the mean wind stress bias. The domain-average surface wind stress is 0.04 N/m2 in the model and 0.06 N/m2 in ASCAT.**

Seasonal variability of the precipitation patterns and their associated large-circulation in the coupled model is generally realistic. Over South America, a marked contrast is observed between austral winter and summer. During austral winter, precipitation maxima are primarily located over the tropical region along the Intertropical Convergence Zone (ITCZ), while the central of the continent experiences dry conditions. In contrast, during austral summer, intense precipitation extends from southern half of the Amazon Basin to northern Argentina, reflecting the southern migration of convection associated with the South American monsoon system - SAMS (Valdes-Pineda et al., 2016). The coupled model reproduces these large-scale seasonal shifts, together with the corresponding changes in sea level pressure patterns and low-level (925 hPa) and upper-level (200hPa) circulation (Figure 6). In summer, low-level winds produce enhanced moisture transport toward the continent, while the upper-tropospheric flow exhibits a well-defined divergent pattern consistent with deep convection activity. During winter, strengthened subtropical high-pressure conditions over the southeast Pacific and changes in the upper-level circulation are consistent with reduced continental convection and a northward displacement of rainfall. The close agreement between the coupled model and ERA5-GPM product shows the ability of the model to realistically represent the seasonal variability of the ocean-atmosphere system over the eastern tropical Pacific and western South America. However, the summer-time precipitation in the Andes is overestimated by the model, probably a consequence of the inadequacy of convective parameterizations in complex topography conditions, even at high resolutions (e.g. Junquas et al., 2018; Saavedra et al., 2020; 2026).

https://doi.org/10.5194/egusphere-2026-3371
Preprint. Discussion started: 18 November 2026
© Author(s) 2026. CC BY 4.0 License.

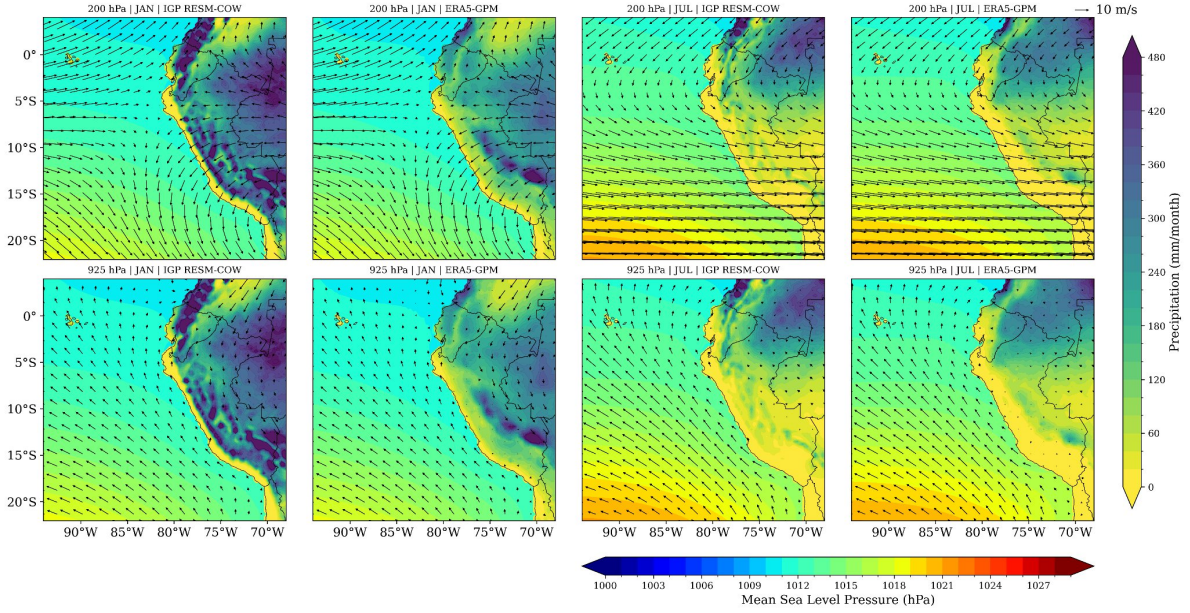



**Figure 6. Mean precipitation for January and July over the 2001-2025 period over South American. Maps are superimposed with upper-level streamlines at 200 hPa (about 12 000 m a.s.l.; Top) and low-level winds vectors at 925 hPa (about 1000 m a.s.l.; Bottom), as well as sea level pressure, derived from the long-term coupled regional ocean-atmosphere model and the GPM (precipitation) and ERA5 (winds and sea level pressure) product.**

The annual cycle of the precipitation is further analyzed over seven representative regions (Figure 7): (1) the northern oceanic region within El Niño 1+2 area (O1: 81.5°-84.5°W / 3.5-6.5°S), (2) the coastal region off Lima (O2: 80°-78° W / 11°13.5° S), (3) the northern coast (C1: 81°-79.3°W / 4°-6°S , (4) the Amazon region (C2: 75°-72° W, 3.5°-5.5° S), (5) central Andes or Mantaro valley (C3: 76°74° W / 11°-13.5° S), and two regions in Ecuador following Ilbay-Yupa et al. (2021): E1 (81° -79° W, 0-2 °S), corresponding to regions R2, R3 and R5 in their Figure 5, and E2 (78° -76° W, 0-2 °S), corresponding to regions R21 and R22. Results from the coupled regional model are compared with observational products, including GPM and, over land, the PISCO product. Over the seven continental regions, the coupled model successfully reproduces the main features of the observed seasonal cycle, including the timing of the wet and dry seasons and the amplitude of the annual modulation. High temporal correlations are found in all coastal land regions (r=0.89-0.91; see Table A.1 in supplementary material), indicating that the model robustly captures the phase of the seasonal cycle across these climatic regions. Over the northern coast (C1), the model represents the sharp austral-summer maximum and the rapid transition toward dry winter conditions, although with a positive precipitation bias. In the central Andes (C3), the strong seasonality is realistically simulated, with maximum precipitation during austral summer and a marked winter minimum. Over the Amazon region (C2), the simulated cycle closely follows the observed evolution, with high precipitation during austral summer and early autumn and reduced precipitation during austral winter, again with a tendency toward overestimation in annual totals. A comparable seasonal evolution is also reproduced over Ecuador regions (E1 and E2), where the model captures the austral-summer precipitation maximum, although with regional biases in precipitation amplitude. Despite these positive amplitude biases, the high correlations and moderate RMSE values indicate that the coupled system realistically represents the seasonal organization of continental precipitation.

For the northern oceanic region within El Niño 1+2 area (O1), the model reproduces the observed seasonal evolution, characterized by a well-defined austral-winter maximum and very low precipitation during the rest of the year. Although

https://doi.org/10.5194/egusphere-2026-3371
Preprint. Discussion started: 18 November 2026
© Author(s) 2026. CC BY 4.0 License.

precipitation is underestimated during the peak months of February and March, the temporal correlation remains high (r=0.92; see Table A.1 in supplementary material), indicating that the model captures the timing and seasonal modulation of precipitation variability. In contrast, over the oceanic region off the central Peruvian coast (O2), the simulated seasonal cycle differs in phase from the observations, leading to an anticorrelated behavior (R = -0.25; see Table A.1 in supplementary material). Although the model does not reproduce the correct timing of the seasonal variability, the simulated precipitation remains of the same order of magnitude as observed.

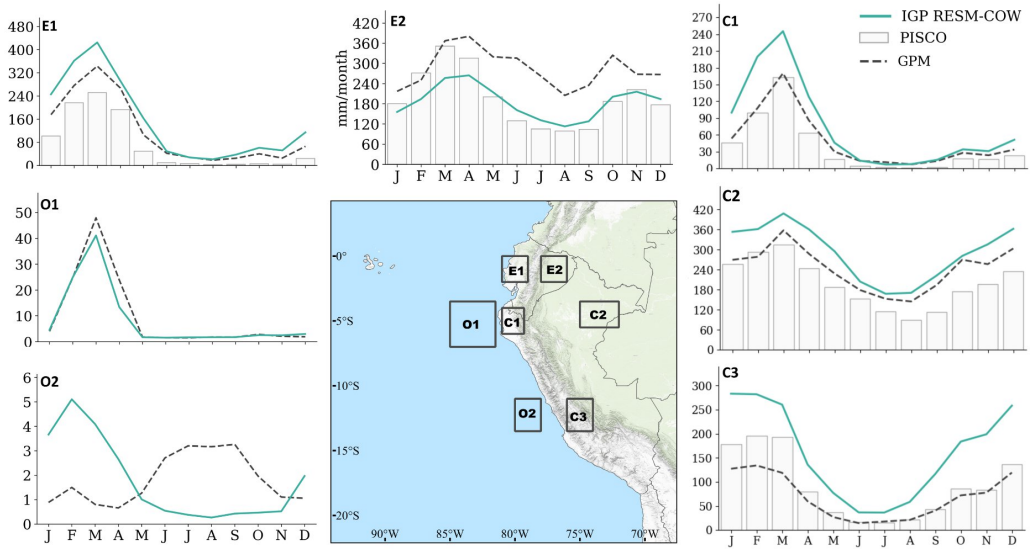



**Figure 7. Annual precipitation cycle computed from the climatology of the coupled ocean-atmosphere model (green line) and the observations of GPM (grey bars) and PISCO (dotted grey lines) products for 2001-2025 period across seven regions: (1) the northern oceanic region within El Niño 1+2 area (O1: 81.5° - 84.5° W, 3.5° - 6.5° S), (2) the coastal region off central Peru (O2: 80° - 78° W / 11° - 13.5° S), (3) the northern coast (C1: 81° - 79.3°W / 4°-6°S , (4) the Amazon region (C2: 75° - 72° W, 3.5° - 5.5° S), (5) central Andes or Mantaro valley (C3: 76° - 74° W / 11° - 13.5° S) and two regions in Ecuador following Ilbay-Yupa et al. (2021): E1 (81° - 79° W, 0-2 °S, corresponding to regions R2, R3 and R5 in their Figure 5, and E2 (78° - 76° W, 0 - 2 °S), corresponding to regions R21 and R22.**

### 3.2 Interannual variability

To assess the realism of the long-term coupled simulation under the interannual variability, we compared the model's monthly outputs with three variables from satellite data sources — SST from the Pathfinder product (AVHRR - Advanced Very High Resolution Radiometer), precipitation from the GPM product, and winds from ASCAT — as well as with one reanalysis data source: 2-m air temperature from the ERA5 product.

https://doi.org/10.5194/egusphere-2026-3371
Preprint. Discussion started: 18 November 2026
© Author(s) 2026. CC BY 4.0 License.

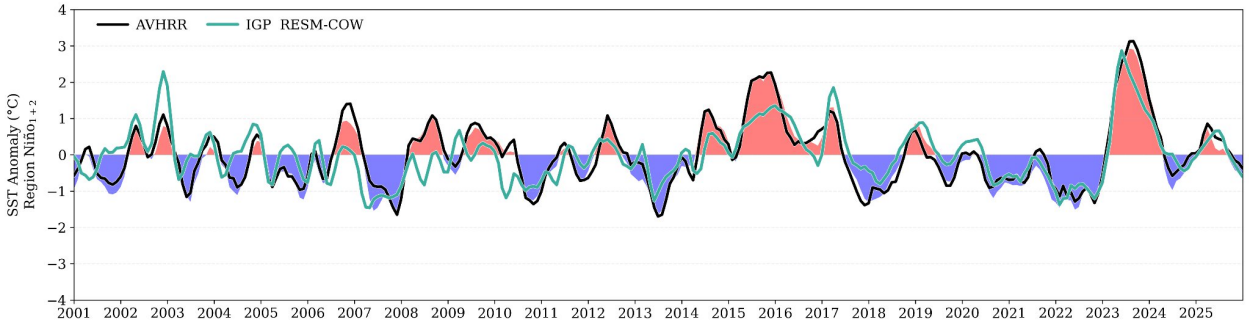



**Figure 8. Time series of the 3-month moving average of the monthly sea surface temperature (SST) anomaly over the Niño 1+2 region calculated from the long-term IGP RESM-COW simulation (green line) and the observed data from the AVHRR satellite product (solid black line) for the period 2001-2025. The ICEN, based on the 3-month running mean SST anomalies in the Niño 1+2 region, is represented with a filled line in red and blue for positive and negative anomalies, respectively.**

Figure 8 presents the time series of the monthly SST anomaly in the Niño 1+2 region, smoothed using a 3-month moving average, for the period January 2001-December 2025. Model results are compared with SST anomalies derived from the AVHRR satellite product and with Coastal El Niño Index (ICEN), which is based on 3-month running mean SST anomalies in the Niño 1+2 region (Takahashi et al., 2014; 2015). The results show that the model presents an acceptable agreement with the observations in terms of large-scale amplitudes; having a correlation between SST anomalies between model-ICEN of 0.8 and model-AVHRR of 0.78 and an RMSE of 0.55°C in both cases, respectively. Furthermore, the simulated intensity is close to that observed during the strong La Niña events of 2007, 2010, 2013 and 2020-2022, the strong El Niño of 2015, and the coastal El Niño of 2017 and 2023.

https://doi.org/10.5194/egusphere-2026-3371
Preprint. Discussion started: 18 November 2026
© Author(s) 2026. CC BY 4.0 License.

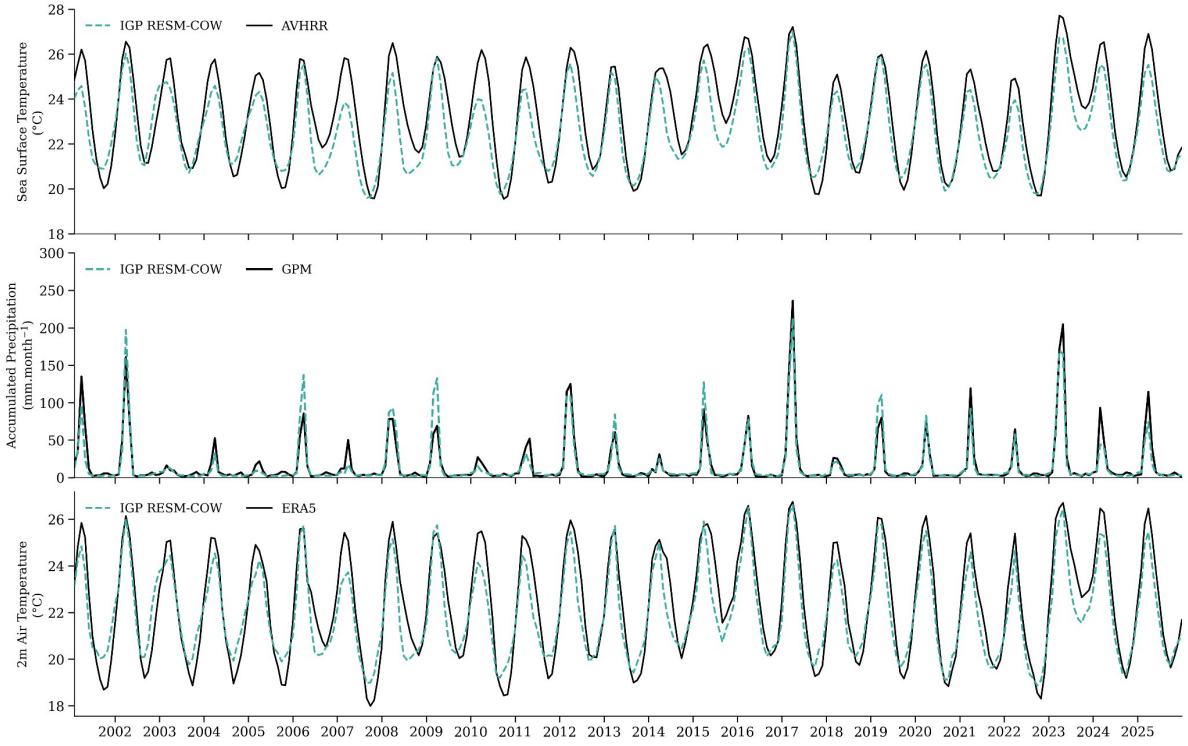



**Figure 9. Monthly mean SST (°C, upper), accumulated precipitation (mm/month, middle) and 2-m air temperature (°C, lower) time series in the Niño 1+2 region calculated from the IGP RESM-COW outputs (green dotted line) and observed data from the AVHRR, GPM and ERA5 product (black lines) over the 2001-2025 period.**

Figure 9 shows a comparison of the monthly mean time series of SST (°C), accumulated precipitation (mm/month), and 2-m air temperature (°C) from the coupled regional model with satellite-based observations (AVHRR, GPM) and ERA5 reanalysis over the Niño 1+2 region for the 2001-2025 period. The simulated and observed time series exhibit a high degree of agreement, with strong linear correlation (ranging from 0.93 to 0.95), and a pronounced, in-phase seasonal cycle characterized by austral summer maxima. The coupled model reproduces both the timing and amplitude of the seasonal signal, as well as the main interannual fluctuations present in the observational datasets.

The quantitative evaluation is extended in Table 2 to seven representative oceanic and continental regions (see Figure 7 for the location of the regions). Overall, the coupled system shows robust skill in reproducing 2-m air temperature variability, with anomaly correlations ranging from 0.50 to 0.82, low RMSE values, and limited systematic biases across most regions. In contrast, precipitation skill exhibits stronger regional contrast. The highest precipitation anomaly correlations are found in the oceanic Niño 1+2 region (O1) and the northern Peruvian coast (C1), where the ocean-atmosphere coupling exerts a strong control on regional variability. Over the coastal region off central Peru (O2), precipitation anomaly correlations remain weak despite relatively low RMSE and bias values, suggesting that the model realistically represents rainfall magnitude while struggling to capture the phase of marine precipitation variability. This likely reflects the strong dependence of offshore precipitation on nonlinear boundary-layer and convection processes that are sensitive to model physics and spatial resolution. At the current atmospheric resolution (30 km), such processes are not explicitly resolved, which limited the model's ability to

https://doi.org/10.5194/egusphere-2026-3371
Preprint. Discussion started: 18 November 2026
© Author(s) 2026. CC BY 4.0 License.

correctly represent the phase and variability of offshore precipitation (e.g., Xie and Philander, 1994; De Szoeke and Xie, 2008; Takahashi and Battisti, 2007; Richter, 2015)

Over the continental interior, particularly over the central Andes (C3) and Amazon region (C2), precipitation biases are larger and anomaly correlations are weaker, indicating persistent difficulties in representing precipitation variability over regions characterized by steep topography and deep convection. Similar limitations are observed over Ecuador's regions (E1 and E2), where the model captures the seasonal cycle but shows moderate skill in reproducing interannual precipitation anomalies. Consistent with previous studies, precipitation simulation over the Andes-Amazon region remains a significant challenge of regional models, with systematic biases and limited interannual variability skill reported (e.g., Gutierrez et al., 2024). Nevertheless, near-surface air temperature remains consistently well represented across all regions, indicating that the coupled system robustly captures the large-scale thermal variability associated with ocean-atmosphere interactions. Overall, the combined evidence from Figure 9 and Table 2 indicates that IGP RESM-COW realistically represents the dominant controls on regional thermal variability, while precipitation processes over complex continental regions remain a key challenge for future model improvement.

Table 2. Skill metrics of the IGP RESM-COW model relative to observations over seven regions during 2001-2025*

| Region | Precipitation | | | 2-m Air Temperature | | |
|---|---|---|---|---|---|---|
| | RMSE | pBIAS | r(anom) | RMSE | BIAS | r(anom) |
| C1 | 53 | 52.1 | 0.83 | 0.75 | -0.44 | 0.77 |
| C2 | 113 | 19.9 | 0.28 | 0.92 | -0.80 | 0.78 |
| C3 | 115 | 132.0 | 0.15 | 0.61 | -0.51 | 0.81 |
| E1 | 81.2 | 30.9 | 0.69 | 0.9 | -0.52 | 0.50 |
| E2 | 133 | -34.7 | 0.35 | 1.04 | -0.93 | 0.70 |
| O1 | 17.5 | -13.4 | 0.91 | 1.06 | -0.49 | 0.74 |
| O2 | 2.9 | -2.2 | 0.11 | 1.03 | 0.53 | 0.60 |

*Precipitation is evaluated using monthly accumulated values, while 2-m air temperature corresponds to monthly means. RMSE and bias metrics are computed from the full monthly series, while interannual variability is evaluated using correlations of monthly anomalies.

To assess the realism of the coupled model below the ocean surface, the analysis is extended to the subsurface thermal variability using ARGO floats deployed in the region. Here, we focus on a representative ARGO float identified by WMO with N° 6903003 (Figure 10). The ARGO record reveals pronounced interannual variability, characterized by significant deepening and shoaling of the upper isotherms, evident in the 15°C, 12° and 10°C surfaces, which reflect changes in the thermocline depth and upper-ocean heat content. A marked deepening of the thermocline is observed during 2023-early 2024, followed by a progressive shoaling in late 2024-2025. This evolution is consistent with the development and decay of the

https://doi.org/10.5194/egusphere-2026-3371
Preprint. Discussion started: 18 November 2026
© Author(s) 2026. CC BY 4.0 License.

2023/2024 El Niño event, during which subsurface heat content buildup and thermocline deepening preceded and characterized the warm phase in the eastern and central Pacific (e.g., Lian et al., 2023; Geng et al., 2024; Peng et al., 2024). The IGP RESM-COW simulation reproduces the main features of this subsurface evolution, capturing both the timing and vertical structure of the isotherm displacements. The model realistically represents the deepening of the upper isotherms and their subsequent recovery, as well as the overall stratification of the upper 500m. Differences remain in the exact depth and sharpness of the thermocline; however, the close correspondence between ARGO and model outputs indicates that the coupled system is able to represent the dominant mechanisms controlling subsurface thermal variability in the region. Results for two other ARGO floats deployed in the region exhibit similar levels of agreement between the IGP RESM-COW simulation and the observations, both in terms of the timing and vertical structure of subsurface thermal variability. Corresponding figures are provided in the Supplementary Material.

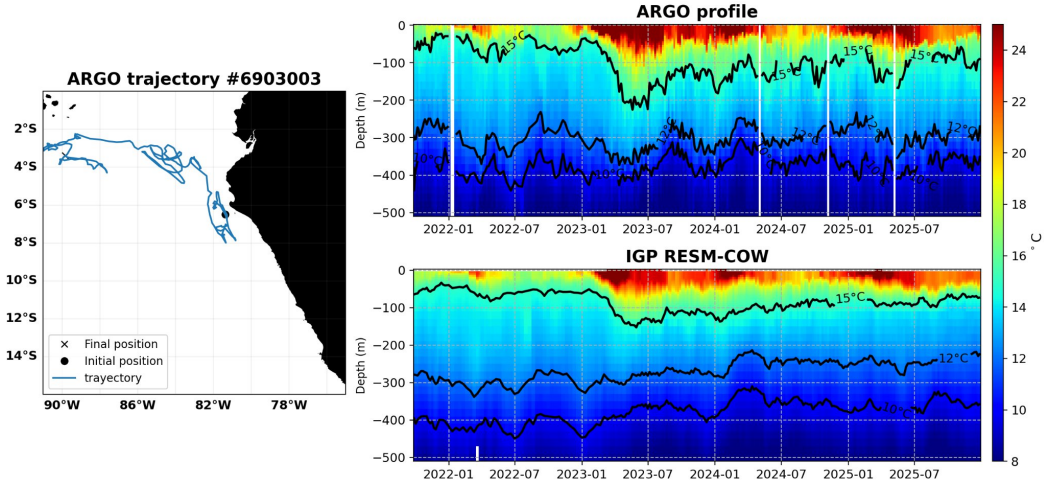



**Figure 10. Trajectory of ARGO float 6903003 (left) and evolution of the upper ocean temperature (top 500 m) along the float path from ARGO observations (Top right) and the long-term IGP RESM-COW simulation (Bottom right) from September 2021 and December 2025. Isotherms of 10°C, 12°C and 15°C are shown as black contour lines.**

To further evaluate the ability of the coupled system to reproduce key atmospheric processes over the region, the analysis is extended to the vertical atmospheric circulation and moisture structure. Figure 11 shows the zonally averaged vertical circulation anomalies and specific humidity anomalies over 80°-85°C for February-April (FMA) 2017 and 2023, corresponding to peak periods of the two latest strongest Coastal El Niño on record (Martinez-Villalobos et al., 2024). The ERA5 reanalysis reveals a well-defined anomalous ascending branch over the coastal eastern Pacific during FMA 2017, extending from the lower troposphere to midlevels and collocated with positive specific humidity anomalies. This vertical structure indicates enhanced low-level moisture convergence and deep convection over the coastal region, consistent with the atmospheric circulation patterns documented for the 2017 coastal El Niño event (e.g., Peng et al., 2019). In FMA 2023, ERA5 shows a similar but weaker vertical overturning structure, characterized by enhanced low-level moisture and upward motion over the eastern tropical Pacific, together with compensation subsidence to the north. The IGP RESM-COW simulation reproduces the main features of these atmospheric anomalies, capturing both the vertical extent and the meridional structure of anomalous ascent, as well as the associated moisture patterns. The model realistically represents the weakened intensity of the 2023 event relative to 2017, although some differences remain in the magnitude and vertical distribution of the anomalies. Overall, the close correspondence between ERA5 and model outputs indicates that the coupled system is able to represent the dominant atmospheric processes associated with coastal warm events in the region. Moreover, the observed vertical circulation

https://doi.org/10.5194/egusphere-2026-3371
Preprint. Discussion started: 18 November 2026
© Author(s) 2026. CC BY 4.0 License.

anomalies and humidity structures are consistent with previously documented atmospheric response to ENSO and coastal warming events, where changes in Walker circulation and air-sea feedbacks modulate vertical motion and moisture convergence over the Pacific (e.g., Bayr et al., 2020; Chen et al., 2016)

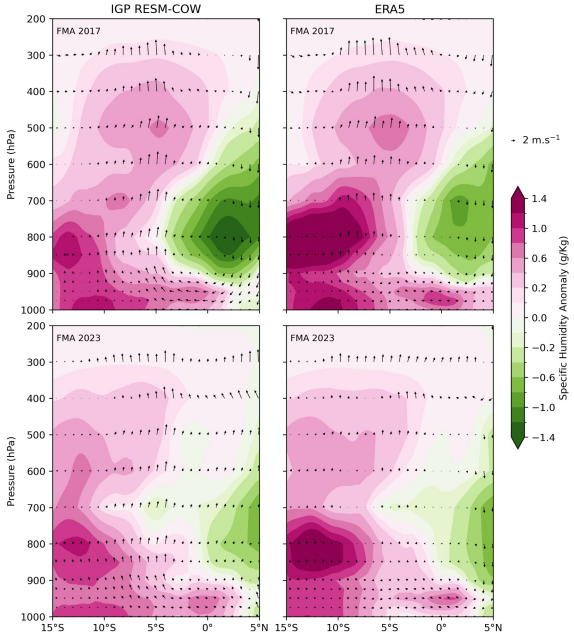



**Figure 11. Zonally averaged vertical atmosphere circulation anomalies (vectors, m/s) and specific humidity (color shading, g/kg) over 80 ° - 85 °W from February-April (FMA) 2017 (Top) and 2023 (Bottom), derived from the long-term IGP RESM-COW simulation (left) and ERA5 reanalysis (right), relative to the 2001-2025 climatological mean.**

## 3.3 Forecast skill

### 3.3.1 Niño 1+2 forecast skill

To evaluate model performance in the Niño 1+2 region, daily outputs from the 7-month forecasts were compared with the AVHRR SST product (Figure 12). The figure shows the temporal evolution of SST from forecasts initialized under different initial conditions between September 2022 and June 2025. The observed AVHRR data exhibit variability ranging from approximately 18.5°C to 29°C, with maxima around April 2023, March 2024 and March-April 2025, followed by a progressive cooling that reaches a minimum during September-October of the subsequent year. Overall, the forecasts remain close to the observed seasonal cycle, even at long lead times, indicating limited initialization shock and a dynamically consistent coupled system. In detail, however, a spread around the seasonal cycle is evident, with differences in both amplitude and timing of extrema, and some forecasts tending to underestimate or overestimate the observed values. The correlation coefficient (R=0.9) and RMSE (1.1°C) computed over the full forecast period primarily reflect the model's ability to reproduce the dominant seasonal cycle. Therefore, these metrics should be interpreted with caution, as they do not fully represent predictive skill beyond climatology variability.

https://doi.org/10.5194/egusphere-2026-3371
Preprint. Discussion started: 18 November 2026
© Author(s) 2026. CC BY 4.0 License.

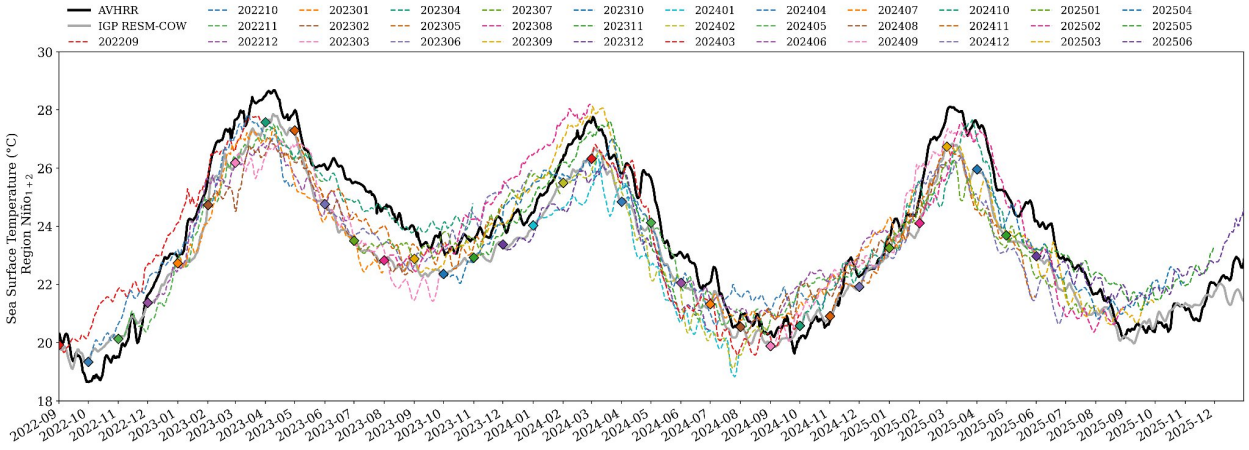



**Figure 12. SST (°C) time series averaged over the Niño 1+2 region from daily forecasts of the coupled model initialized between September 2022 and June 2025 (colored dashed lines). The forecasts are plotted for different initial conditions (see color code on top of the panel). Observations from the AVHRR are shown in black, and the IGP RESM-COW model in the long-term coupled simulation is shown in grey.**

To better assess predictive skill beyond the seasonal cycle, Figure 13 presents monthly SST anomalies in the Niño 1+2 region relative to the 2001-2025 climatology. The forecast captures the onset, development, and decay of the 2023-2024 Coastal El Niño event, although differences in amplitude and timing become more evident at longer lead times. Agreement between forecasts and observations is generally higher during the first three months of prediction, when the model more accurately reproduces the phase and magnitude of SST anomalies. At longer lead times, a larger spread among forecasts develops, reflecting increasing uncertainty in anomaly evolution. Nevertheless, the forecast consistently reproduces the positive SST anomalies associated with the event, indicating meaningful predictive skill at seasonal timescales.

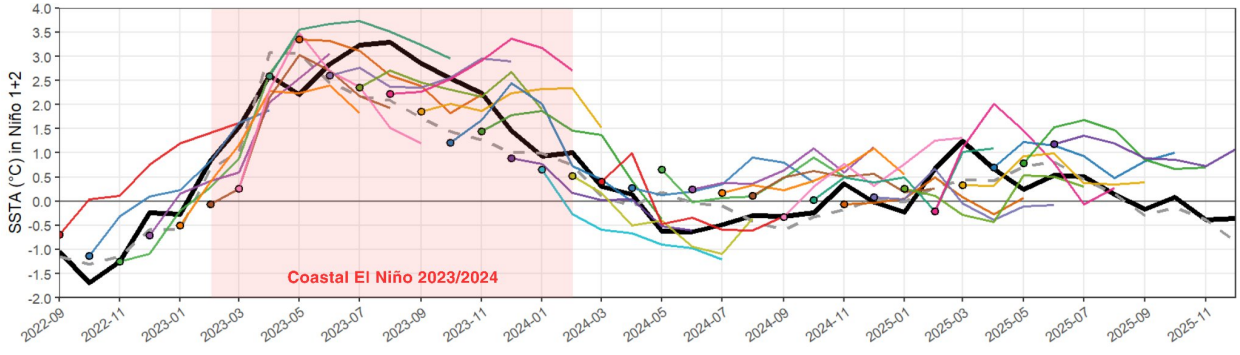



**Figure 13. Monthly SST (°C) anomalies time series averaged over the Niño 1+2 region from daily forecasts of the coupled model initialized between September 2022 and June 2025 (colored solid lines). Observations from the AVHRR are shown in a solid black line, and the IGP RESM-COW model in the long-term diagnostic coupled simulation is shown in a dashed grey line. The colored dots indicate the initialization times of the forecasts. Anomalies are computed relative to the 2001–2025 climatology.**

Forecast performance over the Niño 1+2 region is further quantified using Pearson correlation coefficient (R), anomaly correlation (Ra), anomaly root mean square error (RMSEa) and bias (BIAS) computed from monthly mean SST as a function

https://doi.org/10.5194/egusphere-2026-3371
Preprint. Discussion started: 18 November 2026
© Author(s) 2026. CC BY 4.0 License.

of forecast lead time (Table 3). SST anomalies are defined relative to mean climatology over the period 2001-2025. The coupled model exhibits very high correlation with the observations for the full SST signal, with R remaining above 0.87 for all lead times and reaching values close to 0.98 at lead 0, indicating a robust representation of the seasonal variability. Anomaly correlations (Ra) remain positive throughout the 7-month forecast window, although with lower magnitudes (ranging between 0.76 and 0.86) and a general decrease with lead time, reflecting a gradual loss of phase accuracy in the prediction of SST anomalies. RMSEa values range between 0.69 °C and 0.85°C, showing relatively limited growth with lead time and indicating that the amplitude of SST anomaly variability is reasonably well constrained. Biases are consistently negative across all leads, with magnitudes smaller than 0.7°C and decreasing toward longer lead times, suggesting a modest cold bias that does not substantially degrade forecast skill. Overall, these metrics confirm that SST predictability in the Niño 1+2 region is primarily limited by phase errors in anomalies rather than by systematic amplitude or mean-state errors.

Table 3. Pearson correlation coefficient (R), anomaly correlation (Ra), anomaly root mean square error (RMSEa) and Bias (BIAS) from monthly mean sea surface temperature (SST) data over the Niño 1+2 region*

| Lead | R | Ra | RMSEa | Bias |
|---|---|---|---|---|
| 0 | 0.98 | 0.86 | 0.69 | -0.76 |
| 1 | 0.96 | 0.83 | 0.75 | -0.51 |
| 2 | 0.94 | 0.82 | 0.77 | -0.44 |
| 3 | 0.93 | 0.82 | 0.73 | -0.46 |
| 4 | 0.87 | 0.78 | 0.79 | -0.47 |
| 5 | 0.88 | 0.77 | 0.83 | -0.42 |
| 6 | 0.89 | 0.76 | 0.85 | -0.41 |

*Statistics are reported for both monthly SST values and SST anomalies derived from observed (AVHRR) and forecasted SSTs from the RESM-COW IGP for the seven months of forecast, considering different initial conditions (from C.I. = 202209 to C.I. = 202506). Bold values of R indicate statistically significant correlations at the 95% confidence level ($p < 0.05$).

Finally, to provide an compact assessment of forecast performance, the skill of SST predictions in the Niño 1+2 region is evaluated using the RMSE computed from monthly mean SST and the anomaly correlation coefficient (ACC) computed from monthly SST anomalies as a function of lead time (Figure 14). Monthly SST anomalies are defined relative to a monthly climatology calculated over the period 2001-2025, without detrending. Anomalies for each system (IGP RESM-COW and CFS) and for the observations are computed relative to their own monthly climatologies over this period, so that each system's mean bias is removed in the ACC. RMSE and ACC are computed from 34 monthly forecast initializations between September 2022 and June 2025, each integrated for up to seven months. The performance of IGP RESM-COW is assessed against persistence and climatological reference forecasts. The persistence forecast holds the observed conditions at initialization constant throughout the forecast period. Because the RMSE is computed from absolute monthly-mean SST, persistence in the RMSE is absolute SST persistence: the observed SST at the initialization month is kept fixed for every target month, $SST_m^{pers} = SST_{to}^{obs}$ for a forecast initialized at time *to* and verifying in calendar month m. Because the ACC is computed from anomalies, persistence in the ACC is anomaly persistence: the observed SST anomaly at initialization is kept fixed, $SST'^{pers}_m = SST'_{to}$ , where $SST'_{to}$ is the observed SST anomaly at initialization relative to the 2001-2025 climatology. The

https://doi.org/10.5194/egusphere-2026-3371
Preprint. Discussion started: 18 November 2026
© Author(s) 2026. CC BY 4.0 License.

climatological reference forecast is the monthly climatological SST for the corresponding target month, $SST_m^{clim} = \underline{SST}_m^{clim}$ equivalent to assuming a zero SST anomaly; it is therefore shown only for the RMSE, since a constant-anomaly forecast has an undefined anomaly correlation. The results show that the RMSE of the coupled forecasts increases gradually with the lead time, reaching values of approximately 1.3 - 1.4°C at lead 4, and remains substantially lower than that of persistence, which rapidly degrades and exceeds 4°C beyond lead 3. In comparison, the CFS exhibits a higher RMSE than IGP RESM-COW at most lead times and shows a more pronounced error growth, particularly beyond lead 3-4 months. The climatological reference, by contrast, remains constant and provides a lower-bound benchmark. The ACC further demonstrates the added value of the coupled system: IGP RESM-COW maintains positive correlations of SST anomalies up to 3-4 months, with skill generally comparable to or slightly higher than that of CFS, especially at longer lead times. In contrast, persistence skill rapidly decreases and becomes weakly or negatively correlated beyond approx. 3 months. Although ACC exhibits some non-monotonic behaviour at extended leads, the coupled forecasts consistently outperform persistence and are competitive with, or superior to, CFS. Overall, these results indicate that IGP RESM-COW retains meaningful predictive skill for the temporal evolution of SST anomalies on subseasonal-to-seasonal timescales in the Niño 1+2 region. Note that the use of RMSE and ACC relative to persistence and climatological reference is a standard approach for assessing the added value of dynamical SST forecasts (e.g., Jan van Oldenborgh et al., 2005; Mittermaier, 2008; Jin et al, 2018). Persistence provides a particularly stringent benchmark, as it represents the inherent memory of the ocean system, against which true forecast skill must be demonstrated (e.g., Sanchez-Gomez et al., 2024).

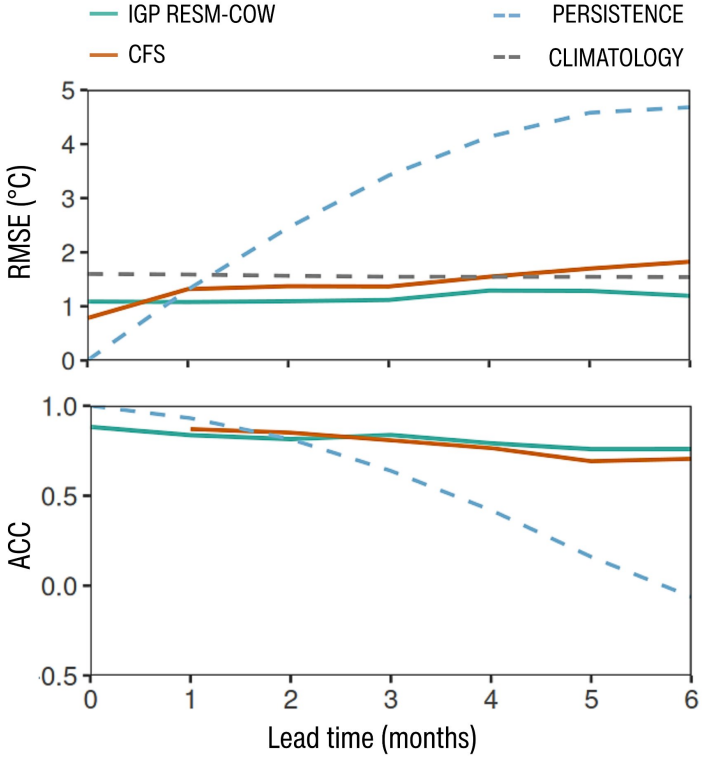



**Figure 14. Root mean square error (RMSE) of monthly mean SST (top) and anomaly correlation coefficient (ACC) of monthly SST anomalies (bottom) in the Niño 1+2 region as a function of lead time. Forecast skill from the IGP RESM-COW coupled model is evaluated using 34 monthly forecast initializations each month between September 2022 and June 2025 and integrated for up to**

https://doi.org/10.5194/egusphere-2026-3371
Preprint. Discussion started: 18 November 2026
© Author(s) 2026. CC BY 4.0 License.

**seven months. Monthly SST anomalies are defined relative to the 2001–2025 monthly climatology, without detrending. Forecast performance of IGP RESM-COW (green solid line) and CFS (orange solid line) is compared with persistence (blue dashed line) and the observed monthly climatology (grey dashed line). RMSE is expressed in °C, while ACC represents the linear correlation between forecasted and observed SST anomalies.**

### 3.3.2 Regional assessment of forecast skill

While the IGP RESM-COW system exhibits skill comparable to CFS for the NINO1+2 index, it is important to assess whether it also captures the realism of the SST anomaly patterns along the Peruvian coast. Spatial averaging over the Niño 1+2 region may obscure compensating effects. Assessing the system's added value at local scales is thus essential. To address this, we evaluate the model skill relative to AVHRR observations at a 1-month and 6-month lead time at each model grid point and compare it with that of CFS (Figures 15).

Overall, both CFS and IGP RESM-COW exhibit comparable correlation patterns at both lead times, with the highest skill north of 15°S. However, correlation values are higher (by ~0.1) off the Piura region in northern Peru (~5°S) for IGP RESM-COW at a 5-month lead time, indicating that the model better captures local coupled air–sea interactions in this region, where a coastal jet is present (Dewitte et al., 2011). This highlights a clear added value of the regional system compared to CFS for preparedness applications.

In terms of forecast errors (Figure 15c–d), differences between CFS and IGP RESM-COW are more pronounced. These reflect limitations of CFS in realistically representing coastal upwelling dynamics, leading to spatially structured errors in the RMSE fields, which show clear spatial structure, with the largest errors in the Niño 1+2 region and along the Peru-Chile coastal upwelling zone in the CFS system. In contrast, the IGP RESM-COW configuration shows reduced RMSE over the southeastern Pacific and more spatially distributed error pattern, indicating an improvement in representation of SST anomaly amplitude in this region. At 6-month lead time, forecast skill decreases across both systems, as indicated by lower ACC values and increased RMSE. This change reflects the gradual loss of predictability with increasing lead time, as the influence of the initial ocean state weakens and internal variability becomes more dominant. Nevertheless, the IGP RESM-COW system maintains lower RMSE than CFS, suggesting a more accurate representation of SST variability at longer lead times.

https://doi.org/10.5194/egusphere-2026-3371
Preprint. Discussion started: 18 November 2026
© Author(s) 2026. CC BY 4.0 License.

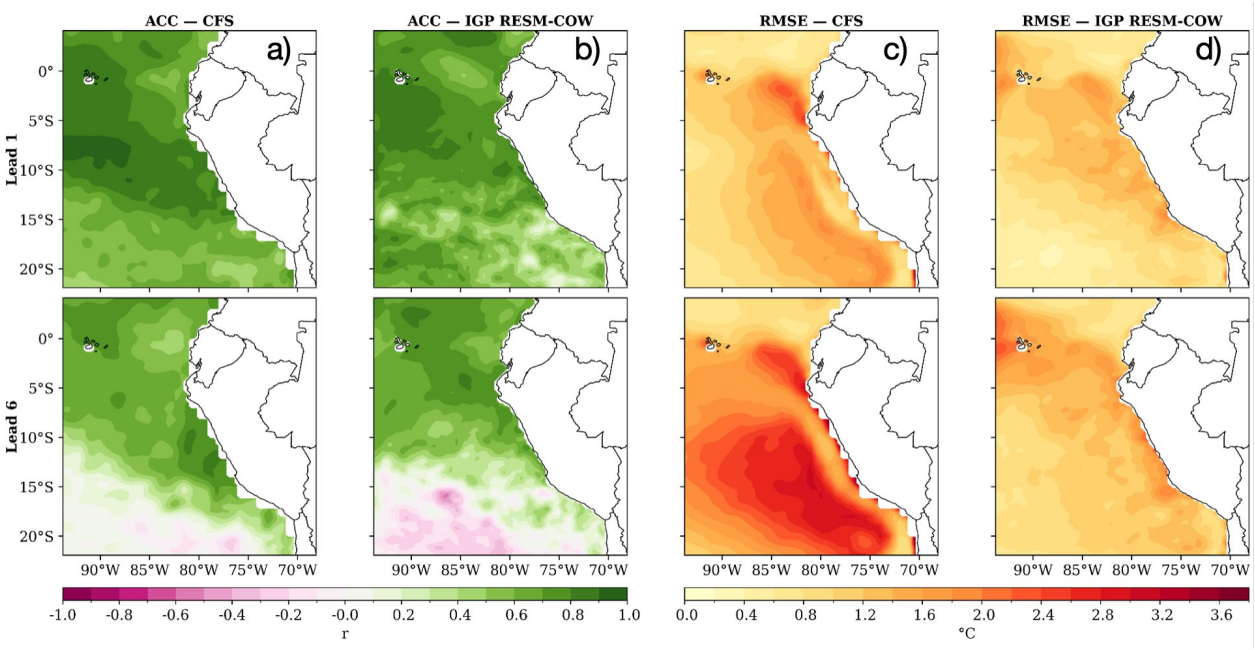



**Figure 15. Spatial distribution of the anomaly correlation coefficient (ACC, a-b) and root mean square error (RMSE, c-d) of monthly sea surface temperature (SST) forecasts for lead times of 1 month (Top) and 6 months (Bottom). Results are shown for the CFS (a, c) and the IGP RESM-COW (b, d) models, both verified against AVHRR observations over the 2022–2025 period using 34 monthly forecast initializations between September 2022 and June 2025.**

On the other hand, the analysis of subseasonal forecast skill of SST anomalies for the IGP RESM-COW model, evaluated against AVHRR observations, shows that a significant level of predictability persists at weekly timescales (Figure 16). ACC values remain above 0.5 over much of the 0°-12°S band up to week 3, indicating that the system captures the evolution of SST anomalies beyond monthly means. Skill is reduced off central Peru (Pisco region), where strong mesoscale activity (Conejero et al., 2020) and the presence of the coastal jet introduce enhanced variability that is difficult to predict. These processes are influenced by both local air-sea interactions and remote equatorial forcing (Dewitte et al., 2011), which likely contribute to the reduced predictability in this region. Consistent with this, RMSE values are largest in coastal jet regions, including Piura and Pisco, where intraseasonal variability of alongshore winds is stronger. Overall, these results demonstrate that the IGP RESM-COW system retains useful skill at subseasonal timescales, particularly in the northern coastal region, supporting its potential application for short-term preparedness.

https://doi.org/10.5194/egusphere-2026-3371
Preprint. Discussion started: 18 November 2026
© Author(s) 2026. CC BY 4.0 License.

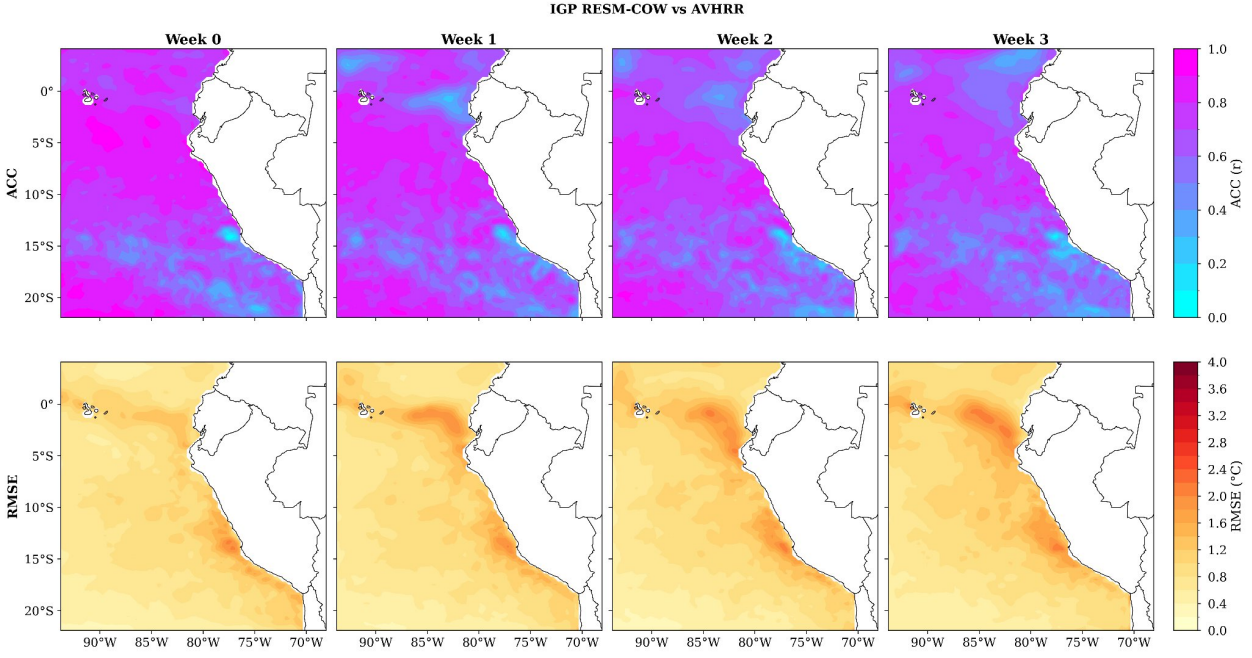



**Figure 16. Subseasonal forecast skill of sea surface temperature (SST) anomalies for the IGP RESM-COW model evaluated against AVHRR observations (September 2022 - June 2025; 34 forecast initializations). (Top) ACC and (bottom) RMSE (°C) computed from weekly-mean SST anomalies for Week 0 (days 1-7), Week 1 (days 8-14), Week 2 (days 15-21), and Week 3 (days 22-end of month). Anomalies were computed by removing a 365-day daily climatology derived from a periodic cubic spline interpolation of the monthly 2001-2025 climatology.**

### 3.3.3 Forecast skill beyond SST

To further evaluate model performance, daily outputs from the 7-month forecasts were compared with the ERA5 air temperature across different regions of the Peruvian territory (Figure 17). The comparison of the temporal evolution of 2-m air temperature over the Niño 1+2 region and the continental areas defined in Section 3.1 (see Figure 7) between the forecasts and ERA5 (Figure 17) shows results consistent with those obtained for SST. In particular, the forecasts reproduce the seasonal variability, capturing the phase of the annual cycle, although differences in magnitude and some dispersion towards the end of the forecast period. In the Amazon region, the representation is more consistent, with the forecasts closely following the observed variability. In contrast, over the Andean region, a larger spread among forecasts is evident, together with difficulties in representing short-term cooling and warming episodes, likely reflecting the limitations of the model over areas of complex topography. Nevertheless, the overall results indicate that IGP RESM-COW provides a reasonable representation of the seasonality and temporal evolution of 2-m air temperature. Forecast performance is more reliable over the coastal and Amazon regions, whereas challenges remain over the Andes, where further improvements are required to enhance predictive skill.

https://doi.org/10.5194/egusphere-2026-3371
Preprint. Discussion started: 18 November 2026
© Author(s) 2026. CC BY 4.0 License.

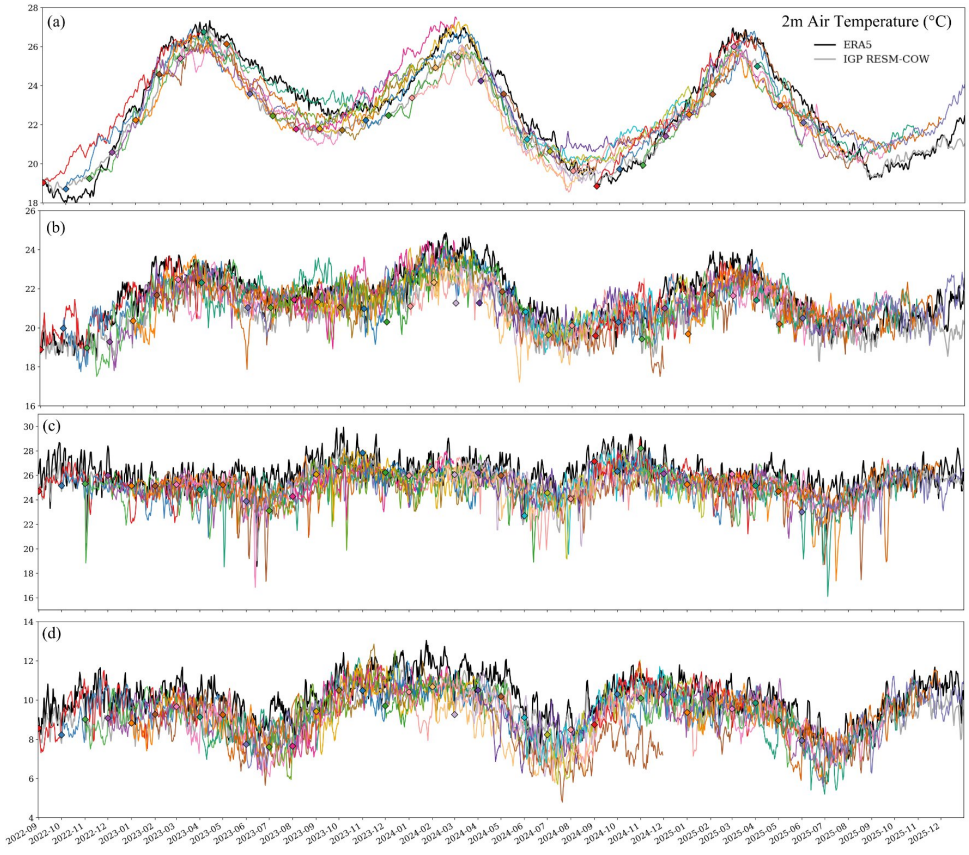



**Figure 17. 2-m air temperature (°C) in the Niño 1+2 region (a) and in three representative areas of the northern coast (81°-79.3° W, 4°-6° S, b), the Amazon region (75°-72° W, 3.5°-5.5° S, c) and the central Andes (76°-74° W, 11°-13.5° S, d) from daily forecasts of the coupled model initialized between September 2022 and June 2025 (colored dots and dashed lines). The forecasts are plotted along their full temporal extent on a common calendar time axis (September 2022-December2025). Observations from the ERA5 are shown in a solid black line, and the IGP RESM-COW model in the long-term coupled simulation is shown in a grey line.**

In addition, the model performance was further evaluated in terms of wind-stress as a main driver of the coastal circulation off Peru. In particular Ekman transport, i.e. $\tau\rho f$ (where $\tau$ is the alongshore wind-stress, $\rho$ the water surface density and $f$ the coriolis parameter), was computed in the Chimbote (80°–78° W, 10°–8° S) and Pisco (78°–76° W, 15°–13° S) regions from the IGP RESM-COW model and ERA5 (Figure 18). The forecasts reproduce the main features of the seasonal cycle, capturing the timing of maxima and minima in agreement with ERA5. However, a reduced amplitude is evident in most forecast members, particularly during periods of enhanced transport. The spread among the forecasts remains relatively limited in Chimbote, whereas larger dispersion is observed in Pisco, consistent with the higher variability of the coastal jet in the region. Furthermore, the model shows reduced skill in capturing short-term fluctuations, especially during transition periods, indicating limitations in representing intraseasonal variability of alongshore winds. Despite these differences, the results suggest that the system provides a reasonable representation of the temporal evolution of coastal wind forcing, although improvements are needed to better capture its amplitude and high-frequency variability.

https://doi.org/10.5194/egusphere-2026-3371
Preprint. Discussion started: 18 November 2026
© Author(s) 2026. CC BY 4.0 License.

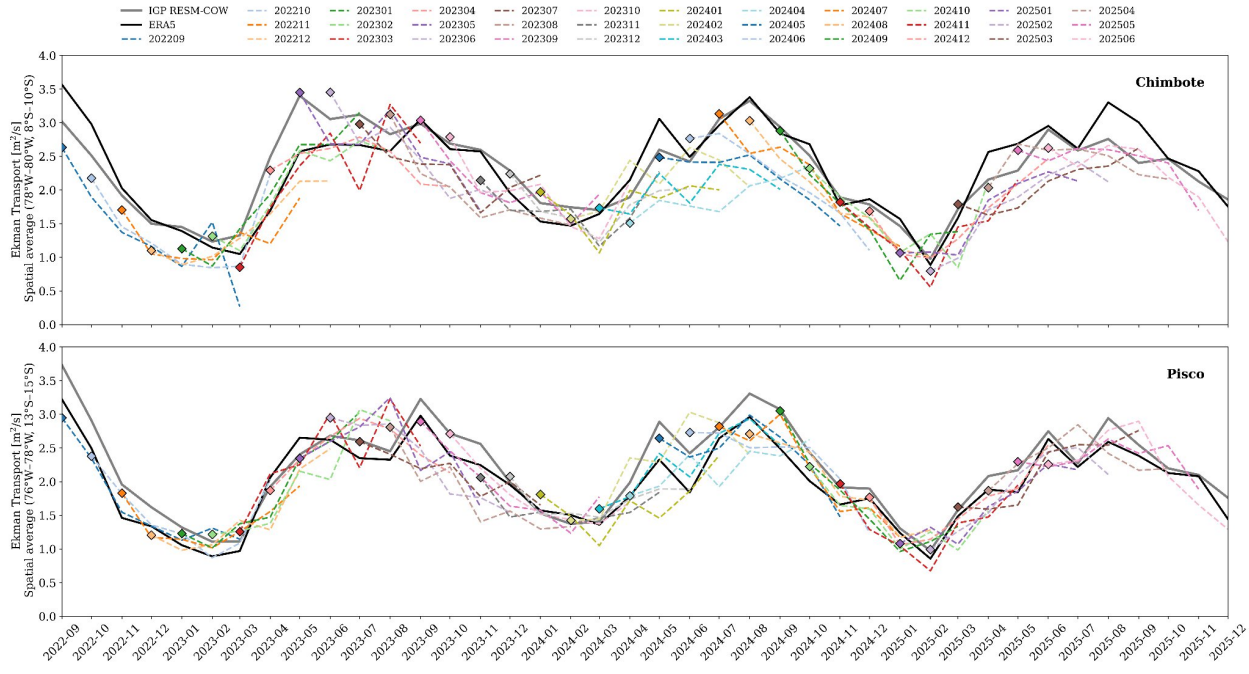



**Figure 18. Monthly-mean Ekman transport ($m^2\ s^{-1}$) off the Peruvian coast in two representative regions: Chimbote (80°–78° W, 10°–8° S; a) and Pisco (78°–76° W, 15°–13° S). The time series are computed from daily wind fields and subsequently averaged to monthly values. The forecasts extend over the same period as in Figure 14. Observations from the ERA5 are shown in a solid black line, and the IGP RESM-COW model in the long-term coupled simulation is shown in a grey line.**

## 4 Conclusions

In this study, we developed and evaluated a regional coupled ocean-atmosphere Earth system model implemented for the eastern tropical Pacific and the Peruvian/Ecuadorian domain (IGP RESM-COW), with the overarching goal of establishing the foundation for a regional forecasting system of extreme climate events in a region highly vulnerable to ENSO variability. The system represents a significant step forward in regional modelling capacity in South America (Cirano et al., 2025), explicitly resolving ocean-atmosphere interactions at spatial scales relevant for a variety of coastal processes in this region (e.g., Dewitte et al., 2011; Dewitte and Takahashi, 2019; Oerder et al., 2024) .

The system is first configured in a long-term coupled simulation spanning 2000-2025, which successfully captures the main large-scale features of the eastern tropical Pacific, including SST gradients, coastal upwelling, and surface wind stress. Over land, the system captures the seasonal cycle and interannual variability of near-surface air temperature, while precipitation skill shows regional contrasts, with reduced performance, generally with overestimation, over areas of complex topography, similar to previous high-resolution modeling studies. Ocean subsurface diagnostics further demonstrate that the model captures key aspects of thermocline variability, including the deepening associated with the 2023-2024 El Niño event (Peng et al., 2025), indicating a physically consistent representation of coupled processes.

In forecast mode, the system shows skill comparable to global products such as CFS in terms of anomalies correlation, while providing clear added value in reducing forecast errors, particularly along the Peruvian coast and in the southeastern Pacific. These improvements appear to be associated with a better representation of SST anomaly amplitude rather than phase,

https://doi.org/10.5194/egusphere-2026-3371
Preprint. Discussion started: 18 November 2026
© Author(s) 2026. CC BY 4.0 License.

highlighting the potential benefits of regional coupling in dynamically complex coastal environments. At subseasonal timescales, the model retains meaningful predictive skill in SST anomalies up to three weeks, particularly in the northern coastal region, demonstrating its potential for short-term preparedness applications. Reduced skill in central Peru is associated with enhanced mesoscale activity and coastal jet variability, which introduce intrinsic limits to predictability. A comparison of SST and wind-driven processes further indicates that SST predictability is sustained even when atmospheric forcing is not fully captured at intraseasonal timescales, reflecting the role of ocean memory in integrating high-frequency variability. This result highlights the importance of coupled ocean-atmosphere dynamics in extending predictability in the region. Overall, the results indicate that IGP RESM-COW provides a physically consistent regional framework for both research and operational applications, offering improved representation of coastal variability and enhanced predictive capability relative to global models.

Future work should focus on quantifying forecast uncertainty and improving the representation of mesoscale and topographic processes, which remain key challenges for regional coupled prediction systems. Now that the system has been established at the IGP, this work is envisioned as part of a sustained institutional effort. Future model development and the quantification of forecast uncertainty could be further advanced through international collaborations and the training of young researchers. A current limitation for a comprehensive assessment of model uncertainty is the limited availability of data from other S2S forecasting centers, particularly for the oceanic component. However, this limitation may soon be alleviated as the S2S community is increasingly evolving toward a more integrated Earth-system perspective, with stronger participation from oceanographers and ocean modeling groups (e.g. SynOBS project, Fujii et al., 2024). Additional effort should also focus on consolidating and extending the evaluation of forecast skill through more comprehensive retrospective analysis, including assessing the added value of the regional system relative to global forecasts such as CFS, as well as the potential non-stationary of forecast skill across periods of contrasting ENSO variability (Sharmila et al., 2023). In addition, the implementation of an ensemble framework will be critical for better quantifying uncertainties associated with natural variability, particularly that arising from mesoscale ocean dynamics. Further developments should also consider the incorporation of process-oriented metrics relevant for decision-making such as upwelling indices (e.g., Ekman versus geostrophic transport, e.g., CUTI index, Jacox et al., 2018), as well as the integration of additional system components, including atmospheric chemistry (e.g., WRF-Chem) and biogeochemical (e.g., Montes et al., 2014) modules, to assess the role of coupled feedbacks on forecast performance and enhance forecast capabilities. Finally, the use of model outputs to train data-driven emulators offers a promising pathway to enhance predictive skill and to extend forecasts toward socio-economic indicators.

## Code and data availability

The source code, model configuration files, experiment settings, post-processing scripts, and processed datasets required to reproduce the simulations and analyses presented in this study are publicly archived in Zenodo as part of the IGP Regional Subseasonal-to-Seasonal (S2S) Ocean-Atmosphere Forecast System for Peru and Ecuador (IGP RESM-COW), version 1 (Montes et al., 2026), https://doi.org/10.5281/zenodo.20516797 .The archive includes the IGP RESM-COW source code and configuration files, MATLAB, R, and Python post-processing scripts, and the processed datasets used to generate the figures, tables, and diagnostics presented in the manuscript. The IGP RESM-COW is based on the open-source Coastal and Regional Ocean COmmunity (CROCO, https://www.croco-ocean.org/) ocean model version 2.0.0, the Weather Research and

https://doi.org/10.5194/egusphere-2026-3371
Preprint. Discussion started: 18 November 2026
© Author(s) 2026. CC BY 4.0 License.

Forecasting (WRF, https://www.mmm.ucar.edu/models/wrf) atmospheric model version 4.0, and the Ocean Atmosphere Sea Ice Soil version 3 Model Coupling Toolkit (OASIS3-MCT, https://oasis.cerfacs.fr/en/downloads/) coupler version 5. The CROCO v2.0.0 source code is archived in Zenodo under DOI:10.5281/zenodo.11036115 (Auclair et al., 2024). WRF v4.0 was released by the National Center for Atmospheric Research (NCAR) on 8 June 2018 and is available through the official WRF source-code release repository (Skamarock et al., 2019). OASIS3-MCT v5.0 was released by CERFACS in December 2021, and its corresponding source code and user guide are available through the official OASIS-MCT repository (Craig et al., 2017; Valcke et al., 2021). The model-specific configuration, coupling, and experiment files used for the simulations presented here are together with the IGP RESM-COW v1 under DOI: 10.5281/zenodo.20516797.

All datasets used in this study, including model input and validation datasets, are publicly available. The Climate Forecast System version 2 (CFSv2) Operational Forecast data used for the variables listed in Table 1 were obtained from the National Centers for Environmental Prediction (NCEP) through the NOAA Climate Forecast System archive hosted by the Registry of Open Data on Amazon Web Service (AWS, https://registry.opendata.aws/noaa-cfs/). Ocean temperature and salinity profiles from the international Argo Program were accessed through the Argo Global Data Assembly Centre (GDAC) using the argos Python library (Maze and Balem, 2020). The ARGO GDAC dataset is available from SEANOE under DOI:10.17882/42182. The exact subset of Argo profiles used in this study is included in the IGP RESM-COW Zenodo archive. Sea surface temperature (SST) observations from the Advanced Very High Resolution Radiometer (AVHRR) were obtained from the NOAA National Centers for Environmental Information (NCEI) NOAA 0.25° Daily Optimum Interpolation Sea Surface Temperature (OISST), Version 2.1, AVHRR-only subset (v02r01), DOI:10.25921/RE9P-PT57 (Huang et al., 2020). The Operational Sea Surface Temperature and Sea Ice Analysis (OSTIA) reprocessed SST product, Global Ocean OSTIA Sea Surface Temperature and Sea Ice Reprocessed (product ID: SST_GLO_SST_L4_REP_OBSERVATIONS_010_011), was obtained from the Copernicus Marine Service and is available under DOI:10.48670/moi-00168. The characteristics and processing of this OSTIA product are described by Worsfold et al. (2024). Atmospheric fields from the fifth-generation European Centre for Medium-Range Weather Forecasts (ECMWF) atmospheric reanalysis (ERA5) were obtained from the Copernicus Climate Data Store. [Monthly averaged single-level variables, including sea-level pressure, near-surface air temperature, and surface winds, are available under DOI:10.24381/cds.17050d7, while monthly averaged pressure-level variables used to evaluate lower- and upper-tropospheric circulation are available under DOI:10.24381/cds.adbb2d47, and ERA5 hourly pressure-level data under DOI:10.24381/cds.bd0915c6]. The ERA5 reanalysis is described by Hersbach et al. (2023). Precipitation estimates from the Global Precipitation Measurements (GPM) mission were obtained from the Integrated Multi-satellitE Retrievals for GPM (IMERG) Early Run daily product, version 07 (GPM_3IMERGDE), distributed by NASA Goddard Earth Sciences Data and Information Services Center (GES DISC), DOI:10.5067/GPM/IMERGDE/DAY/07, Huffman et al. (2023). The Peruvian Interpolated data of the SENAMHI's Climatological and Hydrological Observations precipitation dataset (PISCOp), version 2.1, was obtained from the Servicio Nacional de Meteorología e Hidrología (SENAMHI) through the IRI Data Library. PISCOp v2.1 is described by Aybar et al. (2020), DOI:10.1080/02626667.2019.2649411. The exact PISCOp v2.1 subset used in this study is included in the IGP RESM-COW

https://doi.org/10.5194/egusphere-2026-3371
Preprint. Discussion started: 18 November 2026
© Author(s) 2026. CC BY 4.0 License.

Zenodo archive. Oceanic initial and boundary conditions were obtained from global ocean data-assimilation products distributed by the Copernicus Marine Service and produced by Mercator Ocean International. GLORYS12V1, distributed as the Global Ocean Physics Reanalysis (GLOBAL_MULTIYEAR_PHY_001_030) is available under DOI:10.48670/moi-00021. The PSY4QV3R1 operational ocean analysis and forecast system, distributed as the Global Ocean Physics Reanalysis and Forecast product (GLOBAL_ANALYSISFORECAST_PHY_001_024), is available under DOI:10.48670/moi-00016. Atmospheric initial and boundary conditions were obtained from the National Centers for Environmental Prediction (NCEP) Final (FNL) Operational Global Tropospheric Analyses, available from National Center for Atmospheric Research (NCAR) Research Data Archive under DOI:10.5065/D6M043C6.

## Supplement link

The link to the supplement will be included by Copernicus, if applicable.

## Author contributions

Conceptualization: K.G., B.D., K.T., K.M., V.G. and IM.
Methodology: I.M., B.S., K.T., B.D., V.G., and K.G.
Model configuration: I.M., B.S. and K.G.
Investigation: I.M., B.S., F.C. and K.G.
Formal analysis, validation and visualization: I.M., B.S., F.C., F.C., and R.M
Writing – original draft: I.M.
Writing – review and editing: all authors
Resources and computational: D.G.

## Competing interests

The contact author has declared that none of the author has any competing interests.

## Disclaimer

Copernicus Publications adds a standard disclaimer: “Copernicus Publications remains neutral with regard to jurisdictional claims made in the text, published maps, institutional affiliations, or any other geographical representation in this paper. While Copernicus Publications makes every effort to include appropriate place names, the final responsibility lies with the authors. Views expressed in the text are those of the authors and do not necessarily reflect the views of the publisher.”
Please feel free to add disclaimer text at your choice, if applicable.

https://doi.org/10.5194/egusphere-2026-3371
Preprint. Discussion started: 18 November 2026
© Author(s) 2026. CC BY 4.0 License.

## Acknowledgements

IM, BS, FC, RM, KM, KT would like to acknowledge the Peruvian PPR068 programme "Reducción de vulnerabilidad y atención de emergencias por desastres" for financial support of their work. BD acknowledges supports from ANID (Concurso de Fortalecimiento al Desarrollo Científico de Centros Regionales 2020-R20F0008-CEAZA, COPAS COASTAL FB210021 and Fondecyt Regular 1231174) and CNES (CENDA project). This work was supported by the Scientific Committee on Oceanic Research (SCOR) Working Group 155, funded by national SCOR committees and a grant to SCOR from the U.S. National Science Foundation (Grant OCE-1840868). This study has been conducted using E.U. Copernicus Marine Service Information; https://doi.org/10.3389/feart.2021.698876 and https://doi.org/10.48670/moi-00016.

## Financial support

This research has been supported by the Peruvian PPR068 programme "Reducción de vulnerabilidad y atención de emergencias por desastres", ANID (Concurso de Fortalecimiento al Desarrollo Científico de Centros Regionales 2020-R20F0008-CEAZA, COPAS COASTAL FB210021 and Fondecyt Regular 1231174) and CNES (CENDA project).

## Review statement

The review statement will be added by Copernicus Publications listing the handling editor as well as all contributing referees according to their status anonymous or identified.

## References

Auclair, F., Benshila, R., Bordois, L., Boutet, M., Brémond, M., Caillaud, M., ... & Theetten, S. (2022). Coastal and regional ocean community model. *Zenodo*. https://doi.org/10.5281/zenodo.7415181

Argo (2026). Argo float data and metadata from Global Data Assembly Centre (Argo GDAC). SEANOE. https://doi.org/10.17882/42182

Aybar, C., Fernández, C., Huerta, A., Lavado, W., Vega, F., & Felipe-Obando, O. (2020). Construction of a high-resolution gridded rainfall dataset for Peru from 1981 to the present day. Hydrological Sciences Journal, 65(5), 770–785. https://doi.org/10.1080/02626667.2019.1649411

Bayr, T., Dommenget, D., & Latif, M. (2020). Walker circulation controls ENSO atmospheric feedbacks in uncoupled and coupled climate model simulations. *Climate Dynamics*, *54*(5), 2831-2846.

Bertrand, A., Lengaigne, M., Takahashi, K., Avadí, A., Poulain, F. & Harrod, C. 2020. El Niño Southern Oscillation (ENSO) effects on fisheries and aquaculture. FAO Fisheries and Aquaculture Technical Paper Nº. 660. Rome, FAO. https://doi.org/10.4060/ca8348en

Cai, W., McPhaden, M. J., Grimm, A. M., Rodrigues, R. R., Taschetto, A. S., Garreaud, R. D., Dewitte, B., Poveda, G., Ham, Y.-G., Santoso, A., Ng, B., Anderson, W., Wang, G., Geng, T., Jo, H.-S., Marengo, J. A., Alves, L. M., Osman, M., Li, S., ...

https://doi.org/10.5194/egusphere-2026-3371
Preprint. Discussion started: 18 November 2026
© Author(s) 2026. CC BY 4.0 License.

Vera, C. (2020). Climate impacts of the El Niño–Southern Oscillation on South America. *Nature Reviews Earth & Environment,* 1(4), 215-231. https://doi.org/10.1038/s43017-020-0040-3

Carton, J., Chepurin, G., & Chen, L. (2018). SODA3: A New Ocean Climate Reanalysis. *Journal of Climate*, 31, 6967-6983, doi: 10.1175/JCLI-D-18-0149.1.

Capotondi, A., Wittenberg, A. T., Kug, J., Takahashi, K., & McPhaden, M. J. (2020). *ENSO Diversity. El Niño Southern Oscillation in a Changing Climate, 65–86.* doi:10.1002/9781119548164.ch4

Chen, M., Li, T., Shen, X., & Wu, B. (2016). Relative roles of dynamic and thermodynamic processes in causing evolution asymmetry between El Niño and La Niña. *Journal of Climate*, *29*(6), 2201-2220.

Callahan, C. W., & Mankin, J. S. (2023). Persistent effect of El Niño on global economic growth. *Science*, *380*(6649), 1064-1069.

Cirano, M., Alvarez-Fanjul, E., Capet, A., Ciliberti, S., Clementi, E., Dewitte, B., ... & Veitch, J. (2024). A description of existing Operational Ocean Forecasting Services around the Globe. *State of the Planet Discussions*, *2024*, 1-44.

Carton, J., Chepurin, G., & Chen, L. (2018). SODA3: A New Ocean Climate Reanalysis. *Journal of Climate*, 31, 6967-6983, doi: 10.1175/JCLI-D-18-0149.1.

Chen, L., Ma, Z. G., & Fan, X. G. (2012). A comparative study of two land surface schemes in WRF model over Eastern China. Journal of Tropical Meteorology, 18(4), 445

Craig, A., Valcke, S., & Coquart, L. (2017) Development and performance of a new version of the OASIS coupler, OASIS3-MCT_3.0, Geosci. Model Dev., 10, 3297–3308, https://doi.org/10.5194/gmd-10-3297-2017.

Colas, F., McWilliams, J. C., Capet, X., & Kurian, J. (2012). Heat balance and eddies in the Peru-Chile current system. *Climate dynamics*, *39*(1), 509-529.

Conejero, C., Dewitte, B., Garçon, V., Sudre, J., & Montes, I. (2020). ENSO diversity driving low-frequency change in mesoscale activity off Peru and Chile. *Scientific Reports*, *10*(1), 17902.

Jacox, M. G., Edwards, C. A., Hazen, E. L., & Bograd, S. J. (2018). Coastal upwelling revisited: Ekman, Bakun, and improved upwelling indices for the US West Coast. *Journal of Geophysical Research: Oceans*, *123*(10), 7332-7350.

De Szoeke, S. P., & Xie, S. P. (2008). The tropical eastern Pacific seasonal cycle: Assessment of errors and mechanisms in IPCC AR4 coupled ocean–atmosphere general circulation models. *Journal of Climate*, *21*(11), 2573-2590.

Dewitte, B., Illig, S., Renault, L., Goubanova, K., Takahashi, K., Gushchina, D., ... & Purca, S. (2011). Modes of covariability between sea surface temperature and wind stress intraseasonal anomalies along the coast of Peru from satellite observations (2000–2008). *Journal of Geophysical Research: Oceans*, *116*(C4).

Dewitte, B., Takahashi, K., Goubanova, K., Montecinos, A., Mosquera, K., Illig, S., Montes, I., Paulmier, A., Garçon, V., Purca, S., Flores, R., Bourrel, L., Rau, P., Labat, D., Lavado, W., & Espinoza, J. C. (2014). 9. Las diversas facetas de El Niño y sus efectos en la costa del Perú. En S. González Molina & J.-J. Vacher (Eds.), *El Perú frente al cambio climático* (pp. 125-140). IRD Éditions. https://doi.org/10.4000/books.irdeditions.19877

Dewitte, B., & Takahashi, K. (2019). Diversity of moderate El Niño events evolution: role of air–sea interactions in the eastern tropical Pacific. *Climate Dynamics*, *52*(12), 7455-7476.

Ding, Hui, Matthew Newman, Michael A. Alexander, and Andrew T. Wittenberg (2020) Relating CMIP5 Model Biases to Seasonal Forecast Skill in the Tropical Pacific. *Geophysical Research Letters*, 47(5). https://doi.org/10.1029/2019GL086765.

Echevin, V., F. Colas, D. Espinoza-Morriberon, L. Vasquez, T. Anculle, and D. Gutierrez (2018) Forcings and Evolution of the 2017 Coastal El Niño Off Northern Peru and Ecuador. *Frontiers in Marine Science* 5(367). https://doi.org/10.3389/fmars.2018.00367.

Fujii, Y., Remy, E., Balmaseda, M. A., Kido, S., Waters, J., Peterson, K. A., ... & Chikhar, K. (2024). The international multi-system OSEs/OSSEs by the UN Ocean Decade Project SynObs and its early results. Frontiers in Marine Science, 11, 1476131.

https://doi.org/10.5194/egusphere-2026-3371
Preprint. Discussion started: 18 November 2026
© Author(s) 2026. CC BY 4.0 License.

Gutierrez, R. A., Junquas, C., Armijos, E., Sörensson, A. A., & Espinoza, J. C. (2024). Performance of Regional Climate Model Precipitation Simulations Over the Terrain-Complex Andes-Amazon Transition Region. *Journal of Geophysical Research: Atmospheres*, *129*(1), e2023JD038618.

Heino, M., Puma, M. J., Ward, P. J., Gerten, D., Heck, V., Siebert, S., & Kummu, M. (2018). Two-thirds of global cropland area impacted by climate oscillations. *Nature Communications, 9*(1), Art. 1. https://doi.org/10.1038/s41467-017-02071-5

Hersbach, H., Bell, B., Berrisford, P., Biavati, G., Horányi, A., Muñoz Sabater, J., Nicolas, J., Peubey, C., Radu, R., Rozum, I., Schepers, D., Simmons, A., Soci, C., Dee, D., Thépaut, J-N. (2023): ERA5 monthly averaged data on pressure levels from 1940 to present. Copernicus Climate Change Service (C3S) Climate Data Store (CDS), DOI: 10.24381/cds.6860a573 (Accessed on 15-April-2026)

Hong, S., y Lim, J. (2006). The WRF single-moment 6-class mi-crophysics scheme (WSM6). *Journal of Korean Meteorological* Society,42,129–151.

Huang, B., Liu, C., Banzon, V. F., Freeman, E., Graham, G., Hankins, W., Smith, T. M., & Zhang, H.-M. (2020). NOAA 0.25-degree daily optimum interpolation sea surface temperature (OISST), Version 2.1 [Data set]. NOAA National Centers for Environmental Information. https://doi.org/10.25921/RE9P-PT57

Huffman, G. J., Stocker, E. F., Bolvin, D. T., Nelkin, E. J., Tan, J., & Editor: Savtchenko, A. (2023). GPM IMERG Early Precipitation L3 1 day 0.1 degree x 0.1 degree V07 [Dataset]. NASA Goddard Earth Sciences Data and Information Services Center. https://doi.org/10.5067/GPM/IMERGDE/DAY/07 Date Accessed: 2026-01-06

Ilbay-Yupa, M., Lavado-Casimiro, W., Rau, P., Zubieta, R., & Castillón, F. (2021). Updating regionalization of precipitation in Ecuador: M. Ilbay-Yupa et al. *Theoretical and Applied Climatology*, *143*(3), 1513-1528.

Jacox, M. G., Edwards, C. A., Hazen, E. L., & Bograd, S. J. (2018). Coastal upwelling revisited: Ekman, Bakun, and improved upwelling indices for the US West Coast. Journal of Geophysical Research: Oceans, 123(10), 7332-7350.

Jan van Oldenborgh, G., Balmaseda, M. A., Ferranti, L., Stockdale, T. N., & Anderson, D. L. (2005). Did the ECMWF seasonal forecast model outperform statistical ENSO forecast models over the last 15 years?. *Journal of climate*, *18*(16), 3240-3249.

Jean-Michel, L., Eric, G., Romain, B. B., Gilles, G., Angélique, M., Marie, D., ... & Pierre-Yves, L. T. (2021). The Copernicus global 1/12 oceanic and sea ice GLORYS12 reanalysis. *Frontiers in Earth Science*, *9*, 698876.

Jin, Y., Rong, X., & Liu, Z. (2018). Potential predictability and forecast skill in ensemble climate forecast: a skill-persistence rule. *Climate dynamics*, *51*(7), 2725-2742.

Jin, F. F., Kug, J. S., An, S. I., & Kang, I. S. (2003). A near-annual coupled ocean-atmosphere mode in the equatorial Pacific Ocean. *Geophysical Research Letters*, *30*(2).

Junquas, C., Heredia, M. B., Condom, T., Ruiz-Hernández, J. C., Campozano, L., Dudhia, J., ... & Sicart, J. E. (2022). Regional climate modeling of the diurnal cycle of precipitation and associated atmospheric circulation patterns over an Andean glacier region (Antisana, Ecuador). *Climate Dynamics*, *58*(11), 3075-3104.

Kain, J.S. (2004) The Kain-Fritsch Convective Parameterization: An Update. *Journal of Climate and Applied Meteorology,* 43, 170-181.

Kirtman, B., Power, S. B., Adedoyin, A. J., Boer, G. J., Bojariu, R., Camilloni, I., ... & Young, P. (2014). Near-term climate change: projections and predictability. In: Climate Change 2013: The Physical Science Basis. Contribution of Working Group I to the Fifth Assessment Report of the Intergovernmental Panel on Climate Change [Stocker, T.F., D. Qin, G.-K. Plattner, M. Tignor, S.K. Allen, J. Boschung, A. Nauels, Y. Xia, V. Bex and P.M. Midgley (eds.)]. Cambridge University Press, Cambridge, United Kingdom and New York, NY, USA.

Geng, X., Kug, J. S., Shin, N. Y., Zhang, W., & Chen, H. C. (2024). On the spatial double peak of the 2023–2024 El Niño event. *Communications Earth & Environment*, *5*(1), 691.

https://doi.org/10.5194/egusphere-2026-3371
Preprint. Discussion started: 18 November 2026
© Author(s) 2026. CC BY 4.0 License.

Lagos, P., Silva, Y., Nickl, E., & Mosquera, K. (2008). El Niño–related precipitation variability in Perú. Advances in Geosciences, 14, 231-237. https://doi.org/10.5194/adgeo-14-231-2008.

Lavado-Casimiro, W. & Espinoza, J. C. (2014). Impactos de El Niño y La Niña en las lluvias del Perú (1965-2007). Revista Brasileira de Meteorologia, 29(2), 171-182. https://doi.org/10.1590/S0102-77862014000200003

Lellouche, J. M., Greiner, E., Le Galloudec, O., Garric, G., Regnier, C., Drevillon, M., ... & Le Traon, P. Y. (2018). Recent updates to the Copernicus Marine Service global ocean monitoring and forecasting real-time 1/12◦ high-resolution system. *Ocean Science*, *14*(5), 1093-1126.

Lellouche, J. M., Greiner, E., Le Galloudec, O., Regnier, C., Benkiran, M., Testut, C. E., ... & Drillet, Y. (2018). Mercator Ocean Global High-Resolution Monitoring and Forecasting System. *New Frontiers in Operational Oceanography*, 563-592.

Le Galloude, O., Drévillon, M., Garric, G., Hernandez, F., Lellouche, J.-M., Regnier, C., & Drillet, Y. (2025). Product user manual for the global ocean physical analysis and forecast product GLOBAL_ANALYSISFORECAST_PHY_001_024 (CMEMS-GLO-PUM-001-024). Copernicus Marine Service, Mercator Ocean International. https://documentation.marine.copernicus.eu/PUM/CMEMS-GLO-PUM-001-024.pdf

Lian, T., Wang, J., Chen, D., Liu, T., & Wang, D. (2023). A strong 2023/24 El Niño is staged by tropical Pacific Ocean heat content buildup. *Ocean-Land-Atmosphere Research*, *2*, 0011

Machuca, R., Takahashi, K. y Martínez, A. G.(2014). Impactos económicos de El Niño costero en el sector vivienda a causa de inundaciones en la costa norte del Perú. Boletín técnico: Generación de modelos climáticos para el pronóstico de la ocurrencia del Fenómeno El Niño, Instituto Geofísico del Perú, 1 (12), 4-8.

Martinez-Villalobos, C., Dewitte, B., Garreaud, R. D., & Loyola, L. (2024). Extreme coastal El Niño events are tightly linked to the development of the Pacific Meridional Modes. *npj Climate and Atmospheric Science*, *7*(1), 123.

Maze, G., & Balem, K. (2020). argopy: A Python library for Argo ocean data analysis. *Journal of Open Source Software*, *5*.

McAdam, R., Masina, S., Balmaseda, M., Gualdi, S., Senan, R., & Mayer, M. (2022). Seasonal forecast skill of upper-ocean heat content in coupled high-resolution systems. *Climate Dynamics*, *58*(11), 3335-3350.

McCreary Jr, J. P., & Anderson, D. L. (1991). An overview of coupled ocean-atmosphere models of El Niño and the Southern Oscillation. *Journal of Geophysical Research: Oceans*, *96*(S01), 3125-3150.

Mittermaier, M. P. (2008). The potential impact of using persistence as a reference forecast on perceived forecast skill. *Weather and forecasting*, *23*(5), 1022-1031

Montes, I., Schneider, W., Colas, F., Blanke, B., y Echevin, V. (2011). Subsurface connections in the eastern tropical Pacific during La Niña 1999–2001 and El Niño 2002–2003. *Journal of Geophysical Research: Oceans,* 116(C12), doi:10.1029/2011JC007624.

Montes, I., Dewitte, B., Gutknecht, E., Paulmier, A., Dadou, I., Oschlies, A., & Garçon, V. (2014). High-resolution modeling of the Eastern Tropical Pacific oxygen minimum zone: Sensitivity to the tropical oceanic circulation. *Journal of Geophysical Research: Oceans*, *119*(8), 5515-5532.

Montes, I., Mosquera, K., Luna, M., Gilt, H., Gazen, D., & Woodman, R. (2016). Sistema computacional de alto rendimiento para la simulación de fluidos geofísicos HPC-Linux-Clúster. *Boletín técnico: Generación de información y monitoreo del Fenómeno El Niño,* Instituto Geofísico del Perú, 3(3). https://repositorio.igp. gob.pe/handle/20.500.12816/4663

Montes, I., Segura, B., Castillón, F., Manay, R., Mosquera, K. y Takahashi, K. (2023). Pronósticos experimentales del posible FEN para la Comisión ENFEN con un modelo de Sistema Tierra de alta resolución para el territorio nacional y el Pacífico oriental. Informe Técnico, p. 16.

https://doi.org/10.5194/egusphere-2026-3371
Preprint. Discussion started: 18 November 2026
© Author(s) 2026. CC BY 4.0 License.

Montes, I., Castillón, F., Segura, B., Manay, R., & Campos, F. E. (2026). A Regional Subseasonal-to-Seasonal (S2S) Ocean-Atmosphere Forecast System for Peru and Ecuador. https://doi.org/10.5281/zenodo.20516797

Mosquera, K.: Ondas Kelvin oceánicas y un modelo oceánico simple para su diagnóstico y pronóstico. Boletín Técnico "Generación de modelos climáticos para el pronóstico de la ocurrencia del Fenómeno El Niño", Instituto Geofísico del Perú, 1(1), 4-7. URI: http://hdl.handle.net/20.500.12816/4638, 2014.

Nakanishi, M., y Niino, H. (2006). An Improved Mellor-Yamada Level 3 Model: Its Numerical Stability and Application to a Regional Prediction of Advection Fog. *Boundary-Layer Meteorology,* 119, 397-407. http://dx.doi.org/10.1007/s10546-005-9030-8

Oerder, V., Colas, F., Echevin, V., Masson, S., & Lemarie, F. (2018). Impacts of the mesoscale ocean-atmosphere coupling on the Peru-Chile ocean dynamics: The current-induced wind stress modulation. *Journal of Geophysical Research:* Oceans, 123, 812–833. https://doi.org/10.1002/2017JC013294

Oerder, V., Colas, F., Echevin, V., Masson, S., Lemarié, F., & Renault, L. (2024). Impacts of the mesoscale ocean-atmosphere coupling on the Peru-Chile ocean dynamics: Impact of the thermal feedback. *Journal of Geophysical Research*: Oceans, 129, e2023JC020351. https://doi.org/10.1029/2023JC020351

Ordoñez, J., Paredes, J., Vázquez, R., Llacza, A., Jacome, G., De la Cruz, G., ... & Cabos, W. (2024). Benefits of the coupling in the downscaling the South American climate. *Atmospheric Research*, *305*, 107447.

Peng, Q., Xie, S. P., Wang, D., Zheng, X. T., & Zhang, H. (2019). Coupled ocean-atmosphere dynamics of the 2017 extreme coastal El Niño. *Nature communications*, *10*(1), 298.

Peng, Q., Xie, S. P., Passalacqua, G. A., Miyamoto, A., & Deser, C. (2024). The 2023 extreme coastal El Niño: Atmospheric and air-sea coupling mechanisms. *Science Advances*, *10*(12), eadk8646.

Peng, Q., Xie, S. P., Miyamoto, A., Deser, C., Zhang, P., & Luongo, M. T. (2025). Strong 2023–2024 El Niño generated by ocean dynamics. Nat. Geosci., 18, 471–478.

Penven, P., Echevin, V., Pasapera, J., Colas, F., & Tam, J. (2005). Average circulation, seasonal cycle, and mesoscale dynamics of the Peru Current System: A modeling approach. *Journal of Geophysical Research: Oceans*, *110*(C10).

Penven, P., Cambon, G., Marchesiello, P., Sepulveda, A., Benshila, R., Illig, S., Jullien, S., Le Corre, M., Le Genti, S.l, & G., Morvan. (2024). CROCO tools (2.0). Zenodo. https://doi.org/10.5281/zenodo.11036197

Richter, I. (2015). Climate model biases in the eastern tropical oceans: Causes, impacts and ways forward. *Wiley Interdisciplinary Reviews: Climate Change*, *6*(3), 345-358.

Rivera Tello, G. A., Takahashi, K., & Karamperidou, C. (2023). Explained Predictions of Strong Eastern Pacific El Niño Events Using Deep Learning. *Scientific Reports,* 13 (1), 21150. https://doi.org/10.1038/s41598-023-45739-3.

Saavedra, M., Junquas, C., Espinoza, J. C., & Silva, Y. (2020). Impacts of topography and land use changes on the air surface temperature and precipitation over the central Peruvian Andes. *Atmospheric Research*, *234*, 104711.

Saavedra, M., Junquas, C., Takahashi, K., Silva, Y., Espinoza, J. C., & Sierra, J. P. (2026). Impacts of the future Amazon deforestation on the precipitation over the Peruvian central Andes and related atmospheric features. *Atmospheric Research*, 109016.

Sanchez-Gomez, E., Séférian, R., Batté, L., Berthet, S., Cassou, C., Dewitte, B., ... & Voldoire, A. (2024). Description and evaluation of the CNRM-cerfacs climate prediction system (C3PS). *Journal of Advances in Modeling Earth Systems*, *16*(10), e2023MS004193.

Segura, B. y Montes, I. (2021). Análisis de sensibilidad del sistema acoplado regional COW para el Pacífico sudeste. *Boletín científico El Niño,* Instituto Geofísico del Perú, *8*(2), 12-17.

Shchepetkin, A., & McWilliams, J. (2005). The regional oceanic modeling system: a split-explicit, free-surface, topography-following-coordinate ocean model. *Ocean Modelling* 9, 347–404.

https://doi.org/10.5194/egusphere-2026-3371
Preprint. Discussion started: 18 November 2026
© Author(s) 2026. CC BY 4.0 License.

Sharmila, S., Hendon, H., Alves, O., Weisheimer, A., & Balmaseda, M. (2023). Contrasting El Niño–La Niña predictability and prediction skill in 2-year reforecasts of the twentieth century. *Journal of Climate*, *36*(5), 1269-1285.

Skamarock, W., Klemp, J., Dudhia, J., Gill, D., Liu , Z., Berner, J., Wang, W., Powers, J., Duda, M., Barker, D., y Huang, X. (2019). A Description of the *Advanced Research WRF Version 4*. NCAR Tech. Note NCAR/TN-556+STR, 145 pp. doi:10.5065/1dfh-6p97

Smith, W.H. and Sandwell, D.T. (1997) Global Sea Floor Topography from Satellite Altimetry and Ship Depth Soundings. Science, 277, 1956-1962. http://dx.doi.org/10.1126/science.277.5334.1956

Soriano, E., Mediero, L., & Garijo, C. (2019). Selection of Bias Correction Methods to Assess the Impact of Climate Change on Flood Frequency Curves. *Water,* 11(11), 2266.doi:10.3390/w11112266

Stockdale, T. N., Balmaseda, M. A., & Vidard, A. (2006). Tropical Atlantic SST prediction with coupled ocean–atmosphere GCMs. *Journal of Climate*, *19*(23), 6047-6061.

Sulca, J., Takahashi, K., Espinoza, J.-C., Vuille, M. and Lavado-Casimiro, W. (2018), Impacts of different ENSO flavors and tropical Pacific convection variability (ITCZ, SPCZ) on austral summer rainfall in South America, with a focus on Peru. Int. J. Climatol, 38: 420-435. https://doi.org/10.1002/joc.5185

Takahashi, K., & Battisti, D. S. (2007). Processes controlling the mean tropical Pacific precipitation pattern. Part I: The Andes and the eastern Pacific ITCZ. *Journal of Climate*, *20*(14), 3434-3451.

Takahashi, K., Mosquera Vásquez, K. A., & Reupo, J. (2014). El Índice Costero El Niño (ICEN): historia y actualización. https://repositorio.igp.gob.pe/server/api/core/bitstreams/f272dbdc-959e-44d6-b2d8-3a1d7530e04e/content

Takahashi, K., & Reupo, J. (2015). Índice Costero El Niño (ICEN) con nueva fuente de datos. https://repositorio.igp.gob.pe/server/api/core/bitstreams/d429e84b-f43a-4339-afa3-241ae3c0633d/content

Takahashi, K. (2015). El nuevo sistema de alerta ante El Niño y La Niña Costeros del ENFEN. Boletín técnico: Generación de modelos climáticos para el pronóstico de la ocurrencia del Fenómeno El Niño, Instituto Geofísico del Perú, 2 (3), 9-10.

Takahashi, K., & Dewitte, B. (2016). Strong and moderate nonlinear El Niño regimes. *Climate dynamics*, *46*(5), 1627-1645.

Takahashi, K., & Martínez, A. G. (2017). The very strong coastal El Niño in 1925 in the far-eastern Pacific. *Climate Dynamics*. doi:10.1007/s00382-017-3702-1

Takahashi, K., Karamperidou, C., & Dewitte, B. (2018). A Theoretical Model of Strong and Moderate El Niño Regimes. *Climate Dynamics,* 52 (12), 7477–93. https://doi.org/10.1007/s00382-018-4100-z.

Takahashi, K. (2022). Avances en el conocimiento y la predicción de El Niño y su diversidad en el Perú. *Boletín científico El Niño,* Instituto Geofísico del Perú*, 9* (7), 5-13.

Urbina, B., and Mosquera, K.: Implementación y validación de un modelo océanico multimodal para la región ecuatorial del océano Pacífico. Boletín científico El Niño, Instituto Geofísico del Perú, 7 (1), 13-20. URI: http://hdl.handle.net/20.500.12816/4855, 2020.

Valcke, S., Craig, A., Maisonnave, É., & Coquart, L. (2021). OASIS3-MCT User Guide, OASIS3-MCT 5.0, CERFACS, CERFACS TR/CMGC/21/161.

Valdés-Pineda, R., Valdes, J. B., Diaz, H. F., & Pizarro-Tapia, R. (2016). Analysis of spatio-temporal changes in annual and seasonal precipitation variability in South America-Chile and related ocean–atmosphere circulation patterns. International Journal of Climatology, (8), 2979-3001.

Vitart, F., Robertson, A. W., & Anderson, D. L. (2012). Subseasonal to seasonal prediction project: Bridging the gap between weather and climate. *Bulletin of the World Meteorological Organization*, *61*(2), 23.

Vitart, F., Ardilouze, C., Bonet, A., Brookshaw, A., Chen, M., Codorean, C., ... & Zhang, L. (2017). The subseasonal to seasonal (S2S) prediction project database. *Bulletin of the American Meteorological Society*, *98*(1), 163-173.

https://doi.org/10.5194/egusphere-2026-3371
Preprint. Discussion started: 18 November 2026
© Author(s) 2026. CC BY 4.0 License.



963 Weber, N. J., & Mass, C. F. (2017). Evaluating CFSv2 subseasonal forecast skill with an emphasis on tropical convection.
964 *Monthly Weather Review*, *145*(9), 3795-3815.
965 Worsfold, M., Good, S., Atkinson, C., Embury, O. Presenting a Long-Term, Reprocessed Dataset of Global Sea Surface
966 Temperature Produced Using the OSTIA System. Remote Sens. 2024, 16, 3358. https://doi.org/10.3390/rs16183358
967 Xie, S. P., & Philander, S. G. H. (1994). A coupled ocean-atmosphere model of relevance to the ITCZ in the eastern Pacific.
968 *Tellus A*, *46*(4), 340-350.
969 Xue, Y., Chen, M., Kumar, A., Hu, Z. Z., & Wang, W. (2013). Prediction skill and bias of tropical Pacific sea surface
970 temperatures in the NCEP Climate Forecast System version 2. *Journal of climate*, *26*(15), 5358-5378.
971 Yglesias-González, M., Valdés-Velásquez, A., Hartinger, S.M., Takahashi, K., Salvatierra, G., Velarde, R., et al. (2023).
972 Reflections on the impact and response to the Peruvian 2017 Coastal El Niño event: Looking to the past to prepare for the
973 future. *PLoS ONE* 18(9): e0290767. https://doi.org/10.1371/journal.pone.0290767